ARCHIVIO ISTITUZIONALE
DELLA RICERCA

Alma Mater Studiorum Università di Bologna
Archivio istituzionale della ricerca

Integration of catalytic methane oxy-reforming and water gas shift membrane reactor for intensified pure hydrogen production and methanation suppression over Ce0.5Zr0.5O2 based catalysts

This is the final peer-reviewed author's accepted manuscript (postprint) of the following publication:

Published Version:
Fasolini, A., Mafessanti, R., Abate, S., Gramazio, P., De Maron, J., Centi, G., et al. (2023). Integration of catalytic methane oxy-reforming and water gas shift membrane reactor for intensified pure hydrogen production and methanation suppression over Ce0.5Zr0.5O2 based catalysts. CATALYSIS TODAY, 418, 1-15 [10.1016/j.cattod.2023.114047].

Availability:
This version is available at: https://hdl.handle.net/11585/967029 since: 2024-04-04

Published:

DOI: http://doi.org/10.1016/j.cattod.2023.114047

Terms of use:

Some rights reserved. The terms and conditions for the reuse of this version of the manuscript are specified in the publishing policy. For all terms of use and more information see the publisher's website.

This item was downloaded from IRIS Università di Bologna (https://cris.unibo.it/).
When citing, please refer to the published version.

(Article begins on next page)

15 September 2026

Integration of catalytic methane oxy-reforming and water gas shift membrane reactor for intensified pure hydrogen production and methanation suppression over $Ce_{0.5}Zr_{0.5}O_2$ based catalysts

Andrea Fasolini[a,b], Rodolfo Mafessanti[a,b], Salvatore Abate[c], Pio Gramazio[a,b], Jacopo De Maron[a,b], Gabriele Centi[c], Francesco Basile[a,b]*

[a]Dipartimento di Chimica Industriale "Toso Montanari", Alma Mater Studiorum Università di Bologna, Viale Risorgimento 4, 40136 Bologna, Italy.

[b]Center for Chemical Catalysis - C[3], Alma Mater Studiorum Università di Bologna, Viale Risorgimento 4, 40136, Bologna, Italy.

[c]Department of ChiBioFarAM (Industrial Chemistry), University of Messina, ERIC aisbl and INSTM/CASPE, V.le F. Stagno d'Alcontres 31, Messina 98166, Italy

Corresponding author: Francesco Basile, f.basile@unibo.it

Abstract

The production of pure hydrogen from methane or biomethane is a multistep process that can be intensified by the use of membrane reactors. In this study we have synthetized by microemulsion technique Rh and Pt supported over $Ce_{0.5}Zr_{0.5}O_2$ to be applied to the catalytic methane oxy-reforming and water gas shift (WGS) reaction respectively. At first the reformate produced by the reforming process at 750°C was purified using and hydrogen selective empty Pd-based membrane operated at 400°C. This led to pure hydrogen production but it resulted also in a not-fully exploitation of the membrane performances. Thus, the Pt-based catalyst was loaded in the membrane reactor configuration leading to in situ hydrogen production that helped to increase the separation driving force. The water gas shift reaction downstream oxy-reforming was also studied on the $Pt/Ce_{0.5}Zr_{0.5}O_2$ catalyst and evidenced the consumption of hydrogen by methanation at high H_2/H_2O ratio. Comparing the WGS membrane reactor with a classical fixed bed demonstrated that removing hydrogen led to increased CO conversion over the equilibrium of an analogous fixed bed, higher H_2 yield and suppression of the methanation reaction, even at high inlet H_2/H_2O ratio. Optimizing the reaction conditions allowed to reach high hydrogen recoveries (89%) for the integrated oxy-reforming/membrane water gas shift at high GHSV and without the need of a sweep gas.

Keywords

Pd-based membrane reactor, water gas shift, $Ce_{0.5}Zr_{0.5}O_2$-based catalysts, pure hydrogen production, oxy-reforming, methanation suppression

1. Introduction

Hydrogen is a molecule that will play a crucial role in the transition toward a more sustainable and cleaner scenario [1,2]. The possibility of efficient conversion in electricity through fuel cells, make it a versatile energy storage system and energy carrier for the future, sustainable economy [3]. For this reason hydrogen became part of the "Hydrogen strategy for a climate-neutral Europe", which aims to use green hydrogen to substitute fossil fuels in the energy sector [4]. Hydrogen production from water electrolysis has been mainly addressed as a trending topic on the long term. However, other forms of low carbon hydrogen will be needed on the short term to reduce current emissions and sustain the future development of green hydrogen. Fuel cells will be the main finalizers of hydrogen production, converting it to ready to use electricity. However, pure hydrogen must be produced for such applications as carbon monoxide impurities (> 10 ppm) can poison the Pt catalyst of PEM fuel cells [5]. At date, industrial scale hydrogen is mainly produced by steam reforming, which is an endothermic reaction that occurs between methane (or, seldom, another hydrocarbon) and water to produce synthesis gas (syngas), is a mixture of hydrogen and carbon monoxide (Scheme 1) [6].

$$CH_4 + H_2O \leftrightarrows 3H_2 + CO \qquad \text{(Scheme 1)}$$

The endothermic nature of this reaction, results in processes that need to operate at high temperature (> 850 °C) to gain an acceptable conversion and that shows a high difference in temperature between the catalytic bed and the walls of the reactor. To produce pure hydrogen, syngas must be further processed. The reforming outlet is submitted to the water gas shift reaction (WGS) that consumes carbon monoxide and water to give carbon dioxide and hydrogen (Scheme 2) reducing the CO amount and increasing hydrogen yield.

$$CO + H_2O \leftrightarrows H_2 + CO_2 \qquad \text{(Scheme 2)}$$

The reaction is slightly exothermic and not influenced by pressure. Thus, on an industrial scale high pressures can be employed. However, to reach high conversions, two WGS reactors are

usually needed [7]. The first reactor operates at a higher temperature (300-400°C) and employs cheaper catalysts pursuing most of the CO conversion, while the second one is used to further increase conversion at lower temperatures (200-250°C)[8]. Following the water gas shift reactors, the unreacted CO is completely removed by preferential oxidation (PROXY) which involves the following reactions (Schemes 3 and 4) [9].

$$CO + 0.5\ O_2 \leftrightarrows CO_2 \qquad \text{(Scheme 3)}$$

$$H_2 + 0.5\ O_2 \leftrightarrows H_2O \qquad \text{(Scheme 4)}$$

Finally, carbon dioxide is removed by means of pressure swing adsoption (PSA). Given the high capital cost of the different reactors employed, the system is economically viable only on large scales. The four steps cited above, namely high and low temperature WGS, PROXY and PSA, could be reduced to a single step process if a WGS membrane reactor is employed. This consists in a reactor whose walls are selectively permeable to hydrogen [5,10]. With such a setup a pure hydrogen stream can permeate through the membrane, while the other gases (unreacted carbon monoxide, carbon dioxide, steam and methane) are left in the main stream [11]. Moreover, as hydrogen is constantly removed from the reaction environment, conversions can be increased above the equilibrium that would occur in an analogous fixed bed reactor thanks to the Le Chatelier's principle [12].

Palladium membrane reactors are the most performing systems for these kinds of applications, given the high hydrogen permeability and selectivity of this material [13]. Moreover, Pd is active and stable in the purification of hydrogen form syngas and other components between 350°C and 500°C, which are well compatible with water gas shift operating temperature [5].

Some studies have been conducted on WGS membrane reactors using different catalysts and reaction conditions [5,14–16]. The presence of a membrane reactor allowed to reduce the number of steps for hydrogen purification using both commercial and laboratory-produced catalysts providing high CO conversions and hydrogen yields [5,17–23]. Nevertheless, some investigations are still missing to further favor the development of the WGS membrane reactor technology. Analyzing the current literature it can be noted that: (i) few data are reported regarding the occurrence of methanation reaction in fixed bed compared to membrane reactors [5,20,23]; (ii) some work analyze the membrane reactor performances at low pressures (up to 3 bars) although an increase to 10 bars can increase the hydrogen recovery and membrane performances [5,18,23,24]; an inert sweep gas is often used to favor permeation, decreasing the hydrogen partial pressure at the permeate, but this adds a cost to the process [5,18,20,23];

(iv) most of the works use ideal WGS feeds or simulated feeds, while the combination of lab-scale reforming coupled with WGS membrane reactor is not envisioned [5,21]. Here, these missing concepts were unrevealed by performing the WGS reaction in both fixed bed and WGS membrane reactor both coupled with a reforming reactor which provided the real feed for the catalytic tests. The tests were carried out at different pressures, up to 10 bars and with no sweep gas, and the effect of the membrane reactor configuration on the conversion of CO, hydrogen yield and methane selectivity was unfolded. As purification is driven by the difference in partial pressure between the two sides of the membrane [5], classical steam reforming was not the best option for the coupling with WGS membrane reactors, as the presence of high amount of unreacted steam would dilute hydrogen concentration decreasing the membrane performances. A better suit is found in methane oxy-reforming. This process, already reported by our research group [25–27], combines steam reforming with catalytic partial oxidation, an exothermic reaction that occurs between oxygen and methane to produce syngas (Scheme 5).

$$CH_4 + 0.5O_2 \leftrightarrows 2H_2 + CO \quad (\Delta H^0_{298} = -38 \text{ kJ mol}^{-1}) \qquad \text{(Scheme 5)}$$

When the two processes are combined, the thermal energy needed for the steam reforming is provided by partial oxidation of the energy needed for the steam reforming is given by the exothermic oxidation [25]. Moreover, the process is suitable for small scale operation making the use of bio-methane viable. In addition, oxy-reforming employs oxygen and water in sub-stoichiometric ratios which allows to operate at lower temperatures (750°C) than steam reforming, and avoids product dilution by over-stoichiometric steam, producing a stream rich in hydrogen, which could be fed to an empty membrane, a fixed bed WGS reactor or a WGS membrane reactor operating at 400°C for the purpose of this study. This temperature is optimal for Pd membranes as CO adsorption on Pd occurs below 350°C and reduces permeation while membrane stability lowers over 550°C due to pinhole formation[5]. As all the reagents are added at the reforming inlet and the pressure of the two reactors is the same, this work may help to understand how the operative variables can influence the overall process, a concept that is usually forgotten in literature. Further integration has been carried out by synthetizing and applying the catalysts for the oxy-reforming and WGS reactions. In particular, cerium-based oxides, that showed high activity in both reforming and WGS reactions, have been employed as supports [5,25,28–33]. In particular, previous studies showed that a microemulsion synthetized Rh-$Ce_{0.5}Zr_{0.5}O_2$ catalyst was highly active and stable for the oxy-reforming reaction also thanks to the carbon removal properties of the support synthetized in this way [25]. To avoid carbon formation in the membrane reactor and over the WGS catalyst, this

support was chosen also for the WGS catalyst and impregnated with Pt, an active phase that was selected for its activity and stability toward sintering and carbon formation itself [20,34]. Particular attention was given to show the mechanism of the methanation reaction (Scheme 6) over different catalyst in a WGS fixed bed reactor and the effect that hydrogen removal during the membrane reaction operation has on methane formation compared to a fixed bed reactor.

$$CO + 3H_2 \leftrightarrows CH_4 + H_2O \qquad \text{(Scheme 6)}$$

Finally, the operative conditions of the processes were optimized to maximize hydrogen production and purification. The results of this study uncover the potentiality of the WGS membrane reactor process when coupled with real, variable reaction feeds and help to gather further understand of the methanation reaction mechanism over Pt-$Ce_{0.5}Zr_{0.5}O_2$, which will help to study custom strategy to avoid it in both membrane and fixed bed reactors.

2. Experimental

2.1. Catalyst preparation

The $Ce_{0.5}Zr_{0.5}O_2$ support was prepared following an already reported synthetic procedure [25,35]. The Zr^{4+} (precursor: zirconium (IV) oxynitrate hydrate– $ZrO(NO_3)_2x6H_2O$ – 99.00%, Sigma -Aldrich) and Ce^{3+} (precursor: cerium (III) nitrate hexahydrate – $Ce(NO_3)_3x6H_2O$ – 99.99%, Sigma-Aldrich) were dissolved in water. This aqueous solution was mixed with a solution of n – heptane (solvent, 99.00% – Sigma-Aldrich), hexanol (co-surfactant, 99.00% – Sigma-Aldrich), and a non – ionic surfactant (Triton X-100, 99.00% – Sigma-Aldrich). The obtained microemulsion was mixed with another emulsion of heptane, hexane, Triton X and a tetramethylammonium hydroxide pentahydrate (TMAH = $(CH_3)_4NOHx5H_2O$, 97.00% – SigmaAldrich) aqueous solution. The mixture was stirred for 4 h, then filtrated, washed with methanol, and dried at 120 °C overnight. The obtained powder was finely grinded and calcined at 750 °C at a rate of 2 °C/min and kept at that temperature for 5 h. Metal deposition to obtain the catalyst was pursured by incipient wetness impregnation.

The oxy-reforming catalyst was obtained by impregnation of a Rh precursor (Rh (III) nitrate solution ∼10 wt% Rh in > 5 wt.% in HNO_3 – Sigma Aldrich) aqueous solution to obtain a catalyst with a metallic Rh loading of 2.7%wt/wt. The water gas shift catalyst was obtained by impregnation of a Pt precursor (Tetraammineplatinum(II) nitrate 99.995% – Sigma Aldrich) aqueous solution to obtain a catalyst with a metallic Pt loading of 2.0%wt/wt. After drying at

100 °C for 2 h, the catalysts were calcined at 500 °C (ramp rate of 2 °C/min) for 5 h. Finally, the calcined powders were shaped in pellets with a granularity range between 30-60 mesh.

2.2. Catalyst characterization

To characterize the powders obtained in terms of structure and crystalline phase composition, X – ray diffraction (XRD) analysis was carried out using a Philips PW1050/81 diffractometer equipped with a graphite monochromator in the diffracted beam and controlled by a PW1710 unit (Cu Kα, $\lambda = 0.15418$ nm). A 2θ range from 20° to 80° was investigated at a scanning speed of 40°/h.

Specific surface area was determined using an automatic ASAP 2020 Micromeritics sorptiometer and analyzed using a software operating standard BET and BJH methods. The N_2 gas was a 99.999% pure and all the samples tested were pre-outgasses at 150 °C and 30 mmHg, kept 30 min at this temperature and finally heated up to 250 °C and maintained again at this temperature for 30 min, in order to eliminate all the impurities that can be absorbed on the surface of the sample.

A TEM/STEM FEI TECNAI F20 instrument was used to analyse the morphology and metallic nanoparticles size distribution of the reduced catalysts.

Raman analyses at ambient temperature were carried out with 514 nm Ar^+ laser excitation (Renshaw RM1000 spectrometer) coupled with a Leica DMLM microscope and a CCD camera.

A Micromeritics Autochem 2920 instrument equipped with TCD detector was used to carry out temperature programmed reduction (TPR) and oxidation (TPO) as well as the carbon dioxide temperature programmed desorption (CO_2-TPD). The catalysts were firstly heated to 150°C with flowing He (30 mL/min). After cooling at 50 °C the TPR, TPO or CO_2-TPD were performed. In TPR 30 mL/min of 5% H_2/Ar were sent over the sample, while the temperature was increased up to 950 °C at 10 °C/min, then kept at 950 °C for 30 min. He was then flushed and the temperature was reduced to 50 °C. Then, TPO was performed analogously but using 5% O_2/He (30 mL/min) up to 950 °C.

Temperature programmed desorption of CO_2 (CO_2-TPD) was carried out in the same Micromeritics Autochem II instrument. After the He pre-treatment at 500 °C, the sample was cooled down and saturated at 60 °C with 10% CO_2/He, then purged for 1 h with helium at the same temperature to remove the weakly physisorbed molecular probe. Finally, the temperature

was raised under helium flux (30 mL/min) from 60 °C to 900 °C at 10 °C/min and the desorbed carbon dioxide was detected by the TCD detector.

2.3. Membrane preparation

2.3.1. Pd-based membrane

Asymmetric porous α-Al_2O_3 tubes provided by INOPOR, Germany, were used as substrate for the deposition of Pd-based thin films [36]. The alumina tube had a length of 13.0 cm, an internal diameter of 0.7 cm and an external one of 1.0 cm. It was coated in the inner part with Pd forming a 2 μm thin membrane having a length of 10.0 cm, a diameter of 0.7 cm, that resulted in a membrane area of 21.98 cm^2. The ceramic support was firstly cleaned using purified isopropanol and dried at 120°C for 1 h. A Pd thin film was then deposited on these tubular substrates by EPD (Electroless Plating Deposition) method, consisting of two main consecutive steps: (i) Pd-based nanocrystals (seeds) are created on the membrane surface (seeding or activation step), and then (ii) deposition of a Pd layer occurs by reduction of Pd ions present in an aqueous solution in contact with the inner part of the alumina tube using the electrons generated in the reduction of hydrazine over the Pd-based nanocrystals.

The seeding procedure to deposit Pd-nanocrystals on the inner walls of the alumina tube was the following: preparation of two solutions, i.e., an HCl aqueous solution (0,1N) containing 2wt % $PdCl_2$ (solution A) and an aqueous solution (2M) of hydrazine (solution B). The alumina tube, protecting the external side with Parafilm®, was immersed in solution A for 5 min. After washing with distilled water, the tube was immersed in solution B for 5 min and then washed with distilled water. The latter cycle was repeated eight times. The amount of Pd deposited on the support is commonly in the range 10-12 mg.

Electroless plating of the activated alumina tube was carried out by immerging it into a well stirred plating bath containing Pd salt, EDTA, NH_4OH and hydrazine. The whole system was placed in a thermostated chamber maintained at 30°C, adding 1.6 ml of N_2H_4 (1M) dropwise (rate 200 μL/h). The membrane was kept 8 h under stirring and then washed with distilled water and dried at 110°C (2 h). The chemical composition of the optimized plating bath solution is given in Table 1.

A second Pd membrane was prepared following the procedure described above, then a layer of porous titanium silicalite (TS-1) was deposited by a two-step procedure, the pre-seeding with TS-1-nanocrystals by dip-coating, and a secondary growth. The detailed procedure was

described in a previous work where more details about the preparation, characterization and membrane properties are reported [37].

Table 1. Composition and reaction conditions of the plating bath in the preparation of Pd membrane by Electroless Plating

$PdCl_2$	5 g/l
EDTA	40 g/l
NH_4OH (25%wt.)	290 ml/l
N_2H_4 (1M)	10 ml/l
pH	11
Bath temperature	30 °C
Time	8h

2.3.2. Permeability tests

Permeability tests of membranes were made using a stainless-steel reactor earlier described [38]. The membrane reactor was placed in an electrical furnace and heated to the desired temperature. A K-type thermocouple within the membrane tube was used to control the temperature during the permeation experiments. The gases were introduced into the reactor using a calibrated multi-channel mass-flow controller. The inlet feed was connected to the inner side of the membrane and the permeated gases were measured on the outer side of the membrane, at atmospheric pressure. The pressure in the inner side of the tube was monitored via a digital pressure controller. The permeation behaviour of the membrane was measured with pure H_2 and N_2 at 400°C. Tests were made analysing the permeate flux as a function of time at fixed temperature and transmembrane pressure differential.

A stable behaviour on the permeate flux is typically observed after about half hour, then the pressure differential across the membrane is increased (ΔP in the 0.5–5 bar range) and the permeate flux was monitored again as a function of time-on-stream. The following test protocol was used: (i) first the N_2 permeability at 400°C was evaluated in order to evidence the eventual presence of defects in the Pd membrane; then (ii) the H_2 permeability at the same temperature was determined.

2.3.3. Membrane properties (Permeability tests)

The permeate N_2 flow at 400°C was negligible in a range ΔP in the 0.5–5 bar range, ensuring a defect-free membrane. The permeate side was connected to the microGC Agilent 490 and no N_2 was detected (LOD, Limit of detection 4 ppm). Then, the membrane was tested for H_2 permeability at the same temperature. H_2 permeation results are reported in Figure 1 for both the membranes investigated. Concerning the Pd membrane the results indicate that the permeation rate of H_2 was directly proportional to $\Delta P^{0.5}$ with a permeance, given by the slope in Figure 1, of 32.21 $ml*cm^{-2}*min^{-1}*bar^{-0.5}$. On the other hand, a clear deviation from the linearity is observed for the Pd/TS-1, where a good fitting is obtained with $n=^{0.7}$ [37]. In the latter case the n value affects the H_2 permeance which is lower, 28.19 $ml*cm^{-2}*min^{-1}*bar^{-0.7}$. The good linearity and fitting of the data using a value of n=0.5 indicated that the rate controlling step was the bulk diffusion through the Pd layer. While a different mechanism was observed for the Pd/TS-1 membrane as described in a previous work [37]. Here, the use of Pd/TS-1 membrane is used to avoid the direct contact between the catalyst and the Pd layer, that has been demonstrated to be easily deactivated by forming Pd-Alloy that lower the separation performances of the Pd membrane. In our case the TS-1 is used as a porous protective layer and, although affecting the H_2 permeance, the H_2 permeate flux remained still high. Only a slight decrease is observed for the TS-1/Pd membrane which can be attributed to the resistance of the Pd-TS-1 interface.

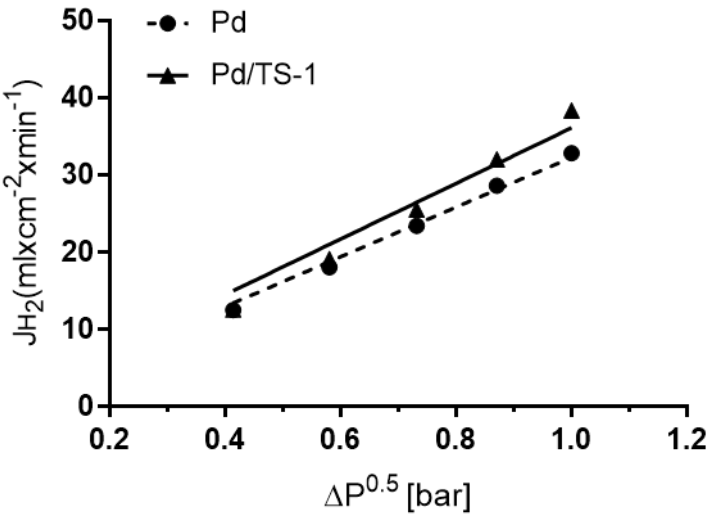

Figure 1. H_2 flux as a function of differential pressure (n=0.5) at 400°C for the Pd- and Pd/TS-1- membrane

2.4. Catalytic tests

2.4.1. Oxy-reforming operation

The oxy-reforming catalytic tests were carried out in a continuous reactor composed of a tubular INCOLOY 800HT tube with a length of 500 mm and an internal diameter 10 mm, which was placed in a furnace. A sliding thermocouple was used to control the temperature of the catalytic bed. The thermocouple could slide inside a stainless-steel tube. The catalyst (0.5 cm^3) was loaded into the reactor and were reduced a 500 ml flow of an H_2/N_2 (10:90 v/v) gas mixture at 750 °C for 12 h**.** Methane and oxygen were fed using mass flow meters and their flux was checked by bubble fluxmeters. A JASCO HPLC pump was used to feed water which was fully vaporized before mixing with preheated O_2. The wet gaseous outlet mixture composed by H_2, CO, CO_2, non-converted CH_4 and vapor was alternatively sent to the WGS unit or analysed by feeding it to a condenser maintained at about 0 °C in order to eliminate water vapor before the gas chromatography. The Micro GC was composed by two columns: a 20 m long MS5A (carrier: N_2), which was used to analyse hydrogen and a 1 m long COx column (carrier: He) which detected CH_4, CO and CO_2. Both modules were equipped with a TCD detector. The CEA-NASA software was used to calculate the outlet composition of the stream at the thermodynamic equilibrium. Table 2 reports the oxy-reforming conditions employed to generate the WGS inlet mixture.

Table 2: Oxy-reforming reaction conditions over Rh-CZO catalyst and produced outlet fed to the WGS reactor, empty membrane or WGS membrane reactor.

Oxy-reforming					**Water Gas shift produced inlet**					
Oven temperature (°C)	**O/C**	**GHSV (h^{-1})**	**Pressure (atm)**	**S/C**	**H_2**	**CO**	**CH_4**	**CO_2**	**H_2O**	**S/DG**
750	0.21	30000	3	1	53	17	9	8	13	0.4
				1.5	49	14	6	8	23	0.8
				2	45	11	5	8	32	1.3
			5	1.5	42	12	9	8	29	1.0
		100000	3	1	42	12	15	9	22	0.6
			5	1	45	11	14	9	21	0.6
				1.5	40	8	12	10	30	1.0
				2	38	7	10	10	35	1.3
840	0.21	100000	10	1.5	45	13	7	8	27	1.0

2.4.2. Hydrogen separation with an empty membrane

The oxy-reforming outlet (Table 2), was firstly fed to an empty Pd membrane, heated at 400°C. Both nitrogen and hydrogen permeability of the membrane was checked before and after each catalytic test to assess the stability of the membrane properties. After reaching 400°C flowing N_2 (≈ 500 mL/min) inside the membrane, the permeate flow was quantified and analysed while increasing the pressure in the retentate side by steps of 0.5 atm to exclude nitrogen permeability. Then, the same procedure was followed feeding an H_2 flow rate of 2250 mL/min, measuring at each pressure the permeate flow rate and the retentate one. The membrane permeability was calculated with the Sieverts-Fick law.

$$J_{H2} = \frac{Pe_{H2}(p^n{}_{H2}, \text{ret} - p^n{}_{H2}, \text{perm})}{\delta}$$

where J_{H2} is the permeated flux (ml*cm^{-2}min^{-2}), Pe_{H2} is the permeability of hydrogen (ml*cm^{-1}*min^{-1}*bar^{-n}), $p_{H2,ret}$ and $p_{H2,perm}$ are the partial pressures of hydrogen at the retentate and permeate side respectively (bar) and δ is the thickness of the palladium layer (cm).

Once the permeability was assessed, hydrogen separation was performed by submitting the oxy-reforming outlet, which was previously analyzed, to the empty membrane. Both retentate and permeate flux were analyzed and quantified with fluxmeter and Micro GC. The membrane performances were evaluated in terms of hydrogen recovery (R_{H2}). which was calculated as follows:

$$R_{H2} = \frac{100 * Flux_{H2}, \text{perm}}{Flux_{H2}, \text{perm} + Flux_{H2}, \text{ret}}$$

2.4.3. Water gas shift reactor and membrane reactor operation

The WGS tests were carried out in a fixed bed reactor or in a membrane reactor to which the oxy-reforming outlet (Table 2) was fed. For both reactors 2,2 cm^3 (3.41 g) of catalyst were charged after mixing with quartz (used to avoid heat transfer problems), so that the catalyst was evenly distributed over the length of the reactor. The reactor was heated through the use of electric ceramic bands controlled by a thermocouple connected to a temperature controller. Table 2 shows the reaction conditions employed. These are the consequence of the oxy-reforming conditions to which they are strictly related. Thus, the WGS feed composition is not the same for all tests but depends on the conditions employed in the oxy-reforming.

The parameter taken in account to compare the oxy-reforming results was methane conversion (X_{CH4}), while those used for WGS were carbon monoxide conversion (X_{CO}), methane selectivity (S_{CH4}), carbon dioxide selectivity (S_{CO2}) and hydrogen yield (Y_{H2}) which were calculated as follows:

$$X_{CH4} = \frac{100 * (Flux_{CH4}, \text{in} - Flux_{CH4}, \text{out})}{Flux_{CH4}, \text{in}}$$

$$X_{CO} = \frac{100 * (Flux_{CO}, \text{in} - Flux_{CO}, \text{out})}{Flux_{CO}, \text{in}}$$

$$S_{CH4} = \frac{100 * (Flux_{CH4}, \text{out} - Flux_{CH4}, \text{in})}{Flux_{CO}, \text{in} - Flux_{CO}, \text{out}}$$

$$S_{CO2} = \frac{100 * (Flux_{CO2}, \text{out} - Flux_{CO2}, \text{in})}{Flux_{CO}, \text{in} - Flux_{CO}, \text{out}}$$

$$Y_{H2} = \frac{100 * (Flux_{H2}, \text{out} - Flux_{H2}, \text{in})}{Flux_{CO}, \text{in}}$$

Moreover, reaction rates of water gas shift and methanation were calculated as follows:

$$r_{WGS} = \frac{moles\ of\ produced\ CO2}{s * moles\ of\ Pt}$$

$$r_{Methanation} = \frac{moles\ of\ produced\ CH4}{s * moles\ of\ Pt}$$

A membrane reactor could be substituted to the WGS fixed bed reactor and fed with the oxy-reforming outlet. A scheme of the laboratory plant is depicted in Figure 2. The reactor was charged with 2.2 cm^3 (3.41 g) of catalyst and heated to the desired temperature.

The catalytic tests in the membrane reactor setup were carried out by feeding the oxy-reforming outlet to the membrane reactor, after it was quantified and analysed with the Micro GC. The permeate and retentate outlets were alternatively analysed with the same instrument and the fluxes were quantified with a fluxmeter. The membrane performances were evaluated in terms of hydrogen recovery (R_{H2}).

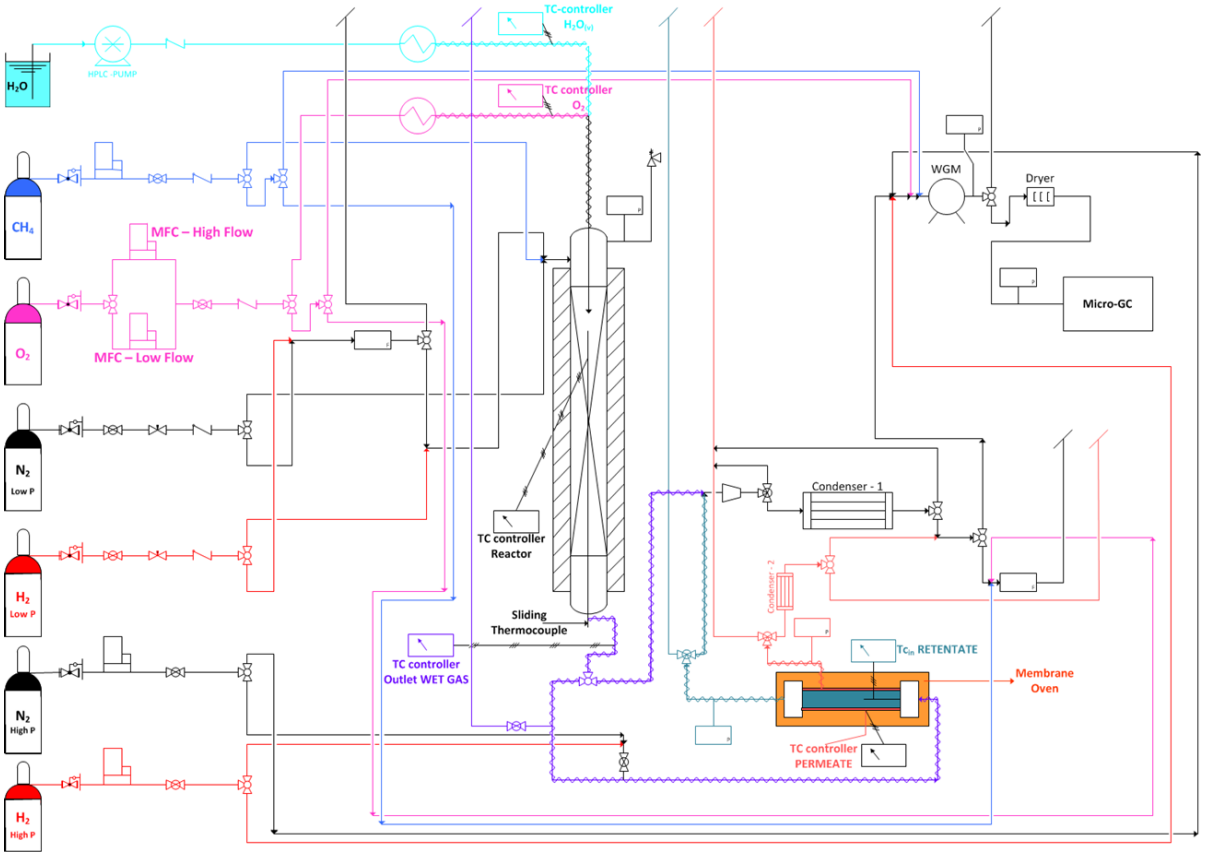

Figure 2: Process flow diagram of the laboratory plant comprising the oxy-reforming reactor followed by the membrane reactor.

3. Results

3.1. Catalyst characterization

A $Ce_{0.5}Zr_{0.5}O_2$ (CZO) mixed oxide was produced by microemulsion synthesis and then impregnated with Rh or Pt to produce the oxy-reforming and water gas shift catalysts respectively (Rh-CZO and Pt-CZO). The microemulsion technique was exploited in previous studies to obtain such support and was selected as it is able to give some peculiar properties to the support [25,35,39–42]. First, it leads to the formation of a $Ce_{0.5}Zr_{0.5}O_2$ mixed oxide with a 1:1 ratio between Ce and Zr as confirmed by XRD analysis shown in Figure 3, without any segregated Ce-rich or Zr-rich phases [25]. This phase has been shown to have a higher oxygen storage capacity compared to other CeZr oxides, a property that helps both catalytic activity and stability [25].

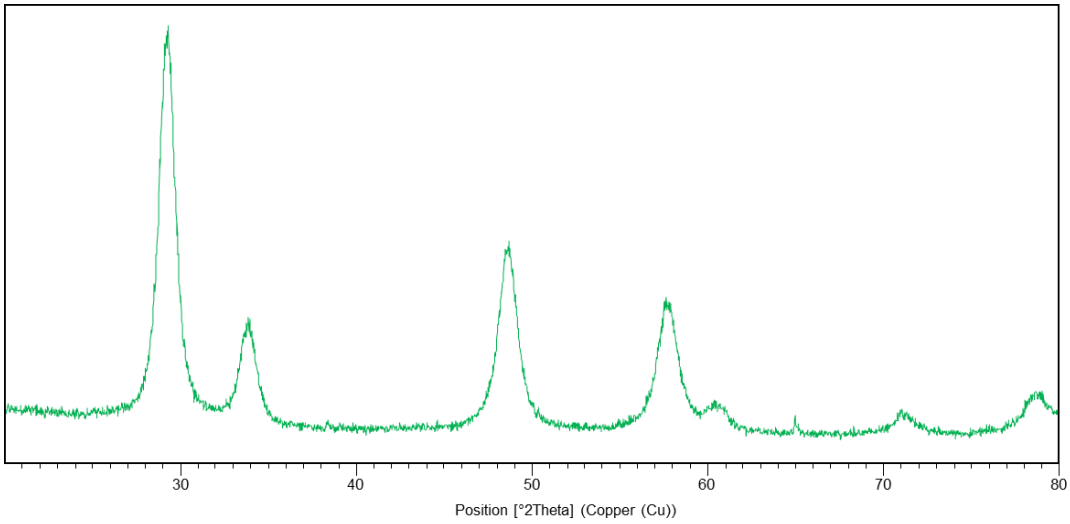

Figure 3: XRD analysis of the $Ce_{0.5}Zr_{0.5}O_2$ obtained by microemulsion.

Second, the microemulsion acts as a templating agent leading to the formation of oxide nanospheres as observed by TEM analysis (Figure 4) with a surface area of 49 m^2/g, which also favours, after incipient wetness impregnation of the metal precursor the dispersion of the metallic active phase and the formation of well-dispersed Rh or Pt nanoparticles, as it was also confirmed by TEM analysis of the Rh and Pt impregnated supports (Figure 4). For these reasons, the Rh and Pt impregnated $Ce_{0.5}Zr_{0.5}O_2$ obtained by microemulsion, were selected as suitable catalysts for the oxy-reforming and water gas shift reactions respectively.

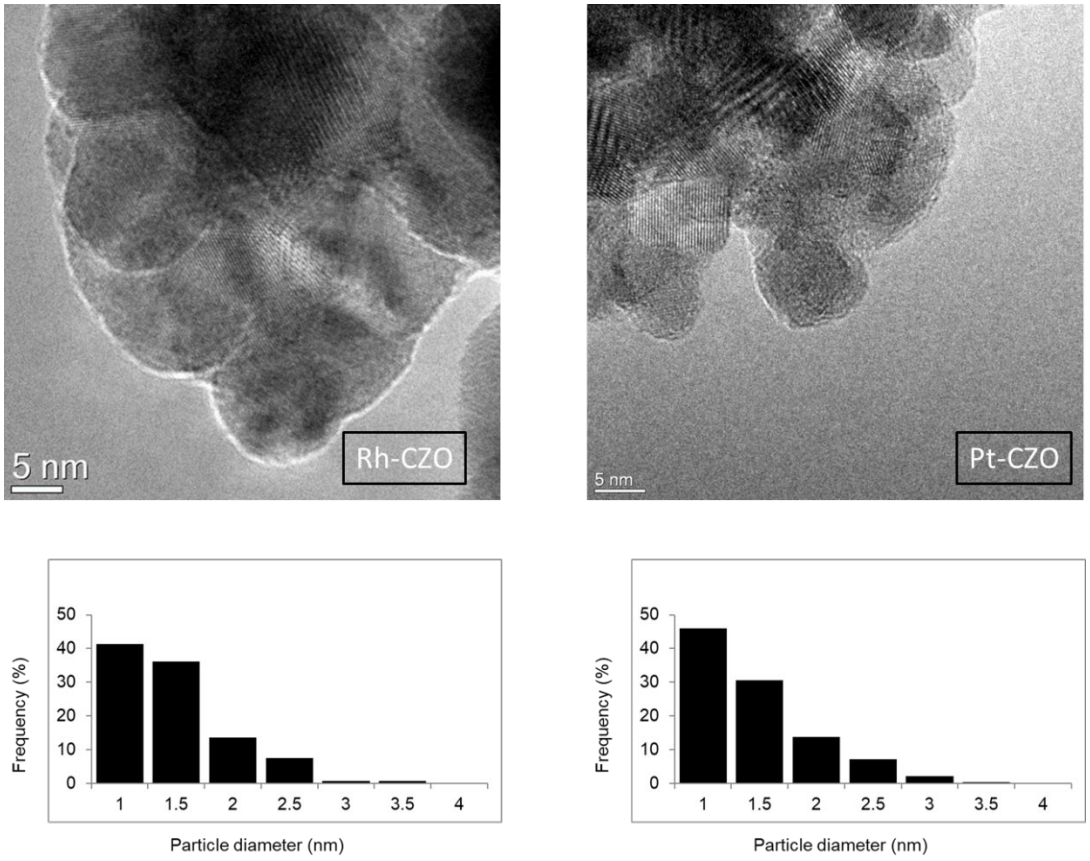

Figure 4: TEM analyses of the Rh and Pt impregnated and reduced on $Ce_{0.5}Zr_{0.5}O_2$ (Rh-CZO and Pt-CZO).

The $Ce_{0.5}Zr_{0.5}O_2$ support was further characterized by Raman analysis, temperature programmed reduction (TPR) and oxidation (TPO) and carbon dioxide temperature programmed desorption (CO_2-TPD) and the results are reported in Figure 5. Raman analysis shows the presence of a main cubic phase, represented by the main band at 465 cm^{-1} and a distorted phase that yields the bands at 300 cm^{-1} and 625 cm^{-1} [43]. This consists in the so-called *t''* phase which is obtained by the distortion of oxygen in a tetragonal fashion inside a cationic cubic structure. The presence of this phase can be obtained when Zr is inserted in the ceria framework [25,43].

Temperature programmed desorption of CO_2 was carried out to probe and quantify the amount of basic sites. The sample showed the presence of a desorption peak at low temperature, which is consistent with what has been reported in literature [44–46], indicative of weak basic sites (0.060 mmol CO_2/g).

Temperature programmed reduction and oxidation were carried out on the bare support as well as the Rh and Pt impregnated catalyst, before reduction. The redox properties of the support

and Rh-based catalysts have been recently reported by our group [42]. In particular, the ceria-based support displays one broad reduction peak in TPR, around 680°C. The presence of a sole reduction peak evidences the homogeneous reducibility of the support thanks to the introduction of Zr and the creation of a mixed oxide phase [42,47]. The reduction temperature decreased upon addition of Rh and Pt. This was consistent with the high reducibility of noble metals, as well as their contribution to the reduction of $Ce_{0.5}Zr_{0.5}O_2$ by hydrogen spillover form the metal to the support surface [25,42,48–50]. Rh-$Ce_{0.5}Zr_{0.5}O_2$ in fact yielded one broad reduction peak around 100°C indicating a homogeneous reduction of Rh oxide and $Ce_{0.5}Zr_{0.5}O_2$ and a smaller one at 250°C resulting from the reduction of less reducible Ce present in the bulk of the sample [42]. On the opposite, the Pt-based catalysts showed the presence of two peaks at 130°C and 438°C respectively. The former is due to the reduction of Pt and surface Ce, while the latter to the reduction of bulk ceria, harder to reduce. Nevertheless, both reductions occur at a lower temperature than the bare support, supporting the occurrence of hydrogen spillover that helped the reduction of the support.

The presence of a sole peak was also observed during TPO of the support as well as of the Rh and Pt based catalysts with all peaks present at low temperature, around 120-130°C and indicating than both metal and support oxidations easily occur.

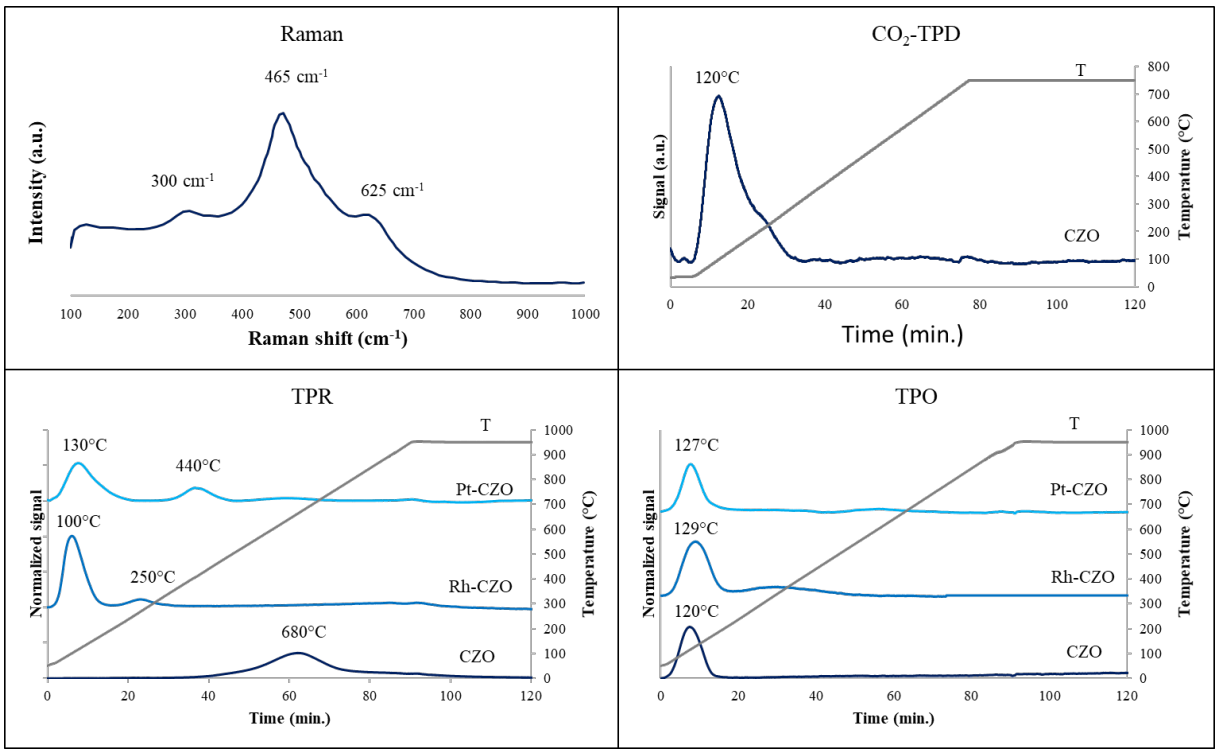

Figure 5: Raman and CO_2 temperature programmed desorption (CO_2-TPD) of the on $Ce_{0.5}Zr_{0.5}O_2$ support (CZO) and temperature programmed reduction (TPO) and oxidation

(TPO) carried out on the bare support (CZO) and after impregnation with Pt and Rh (Pt-CZO and Rh-CZO).

3.2.Oxy-reforming followed by an empty membrane for hydrogen separation.

This work aims to produce pure hydrogen from methane via a two-step process involving an oxy-reforming reactor for methane conversion with oxygen and steam operating at 750°C and a membrane for hydrogen separation at 400°C. The oxy-reforming process was selected for its intrinsic characteristics that met the requirement for efficient hydrogen separation with membrane, which is driven by the difference in hydrogen partial pressure between the retentate (to be separated) and permeate (separated) side. This implies that concentrated and pressurized hydrogen streams lead to more efficient separation. As recalled in the introduction oxy-reforming, nicely suits these requirements, being conducted with low S/C and O/C ratios. Moreover, catalyst optimization and screening were already conducted in previous studies [25,27], which led to the selection of the $Rh/Ce_{0.5}Zr_{0.5}O_2$ catalyst for this process.

At first, an empty membrane was placed after the oxy-reforming unit to purify the hydrogen produced in the reforming step and the outlet streams were analysed both before the membrane (oxy-reforming outlet) and after it (both permeate and retentate sides). Table 3 reports methane conversion given by the oxy-reforming catalyst under different conditions and hydrogen partial pressure depending on total pressure and GHSV obtained analysing the oxy-reforming outlet. The tests were conducted at 3 and 5 bars to allow the obtainment of a hydrogen partial pressure above 1 atm inside the membrane, allowing permeation. In fact, as no sweep gas was used in this work and H_2 pressure at the permeate side is 1 atm at steady state, it must be remembered that values of partial pressures above 1 atm must be present in the retentate to allow permeation. The performances of the reforming process were evaluated by methane conversion and generated hydrogen partial pressure at the membrane inlet while the membrane performances were shown as hydrogen recovery and permeated hydrogen flux.

Table 3: Results of the oxy-reforming catalytic tests carried out at different conditions on $Rh/Ce_{0.5}Zr_{0.5}O_2$ followed by an empty membrane reactor.

Oxy-reforming operative conditions 750°C, S/C=1 O/C=0.21	**X_{CH4} (%)**	**X_{CH4} eq. (%)**	**H_2 partial pressure retentate**	**H_2 partial pressure**	**Pure H_2 flux (ml/min)**	**Hydrogen recovery (%)**

			inlet (atm)	permeate (atm)		
24000 h^{-1}, 3 atm	77	77	1.7	1.0	113	69
100000 h^{-1}, 3 atm	54	70	1.3	1.0	193	38
24000 h^{-1}, 5 atm	67	67	2.6	1.0	134	81
100000 h^{-1}, 5 atm	53	62	2.1	1.0	356	69

The $Rh/Ce_{0.5}Zr_{0.5}O_2$ catalyst employed in the reforming process was able to provide high methane conversion approaching the equilibrium in all the investigated conditions. This allowed to obtain high hydrogen production which resulted in partial pressures as high as 2.6 atm at lower GHSV (24000 h^{-1}) and 5 atm.

The performances of the membrane highly depended on the oxy-reforming operative conditions which affected not only the hydrogen permeation but also the reaction. At 24000 h^{-1} and 3 atm a hydrogen recovery of 69% was obtained as consequence of the high methane conversion favoured by low GHSV and pressure. Increasing the GHSV, lower hydrogen pressure (1.3 atm) was developed as conversion dropped due to low contact times and the reaction was not able to reach the equilibrium. Pure hydrogen flux was higher thanks to the high amounts of fluxes involved but the hydrogen recovery dropped to 38%, with most of the hydrogen being left in the retentate.

Increasing total pressure to 5 atm, raised hydrogen partial pressure which boosted hydrogen recovery to 81% and 69% at 24000 and 100000 h^{-1} respectively. Thus, the best results were obtained at 24000 h^{-1} and 5 atm, showing relatively high conversion and hydrogen recovery. However, at 5 atm, the retentate hydrogen partial pressure at the retentate end of the membrane was 1.00 under all conditions, which was equal to that at the permeate side. As separation is driven by the difference between these two values this indicates that permeation occurred at its maximum extent and that, probably, this value was reached before the membrane exit. This suggests that part of the membrane was inactive and did not contribute to separation as it was not subjected to any driving force. Thus, hydrogen production was holding back hydrogen purification due to a relatively low hydrogen concentration compared to the highly efficient separation performances of the membrane.

Increasing the oxy-reforming catalyst activity, hence hydrogen production in that step, is not a viable option to raise permeation because the conversion already reached the equilibrium under

the best conditions. Nevertheless, the Pd membrane operates at 400°C which is an ideal temperature for the WGS reaction.

For this reason, it was decided to load the membrane with a water gas shift catalyst, in a membrane reactor (MBR) configuration, to concurrently increase hydrogen production and separation.

3.3. Water gas shift reaction in a fixed bed reactor

The fixed bed reactor was charged with Pt-CZO, which was selected as the WGS catalyst. The effect of GHSV, H_2O/CO and total pressure was studied. The effect of the H_2O/CO ratio was investigated at various conditions and showed significantly different results based on the GHSV and the pressure employed. It must be noted that steam is fed to the reforming reactor and not directly to the WGS one. Thus, the H_2O/CO depends on the different S/C (H_2O/CH_4) fed to the oxy-reforming and the catalytic activity of this process such as steam conversion and CO production. In general, the higher the S/C the higher the H_2O/CO ratio. Moreover, as the methane oxy-reforming inlet flux was kept constant while the steam amount was increased in the tests at different S/C (hence H_2O/CO), the GHSV will be partially increased at higher H_2O/CO, as total flux raised. Figure 6 shows the effect of H_2O/CO at low GHSV (10000-13000 h^{-1}) and pressure (3 atm) and at high GHSV (32000-41000 h^{-1}) and pressure (5 atm) on equilibrium and experimental CO conversion, methane and carbon dioxide selectivities and hydrogen yield.

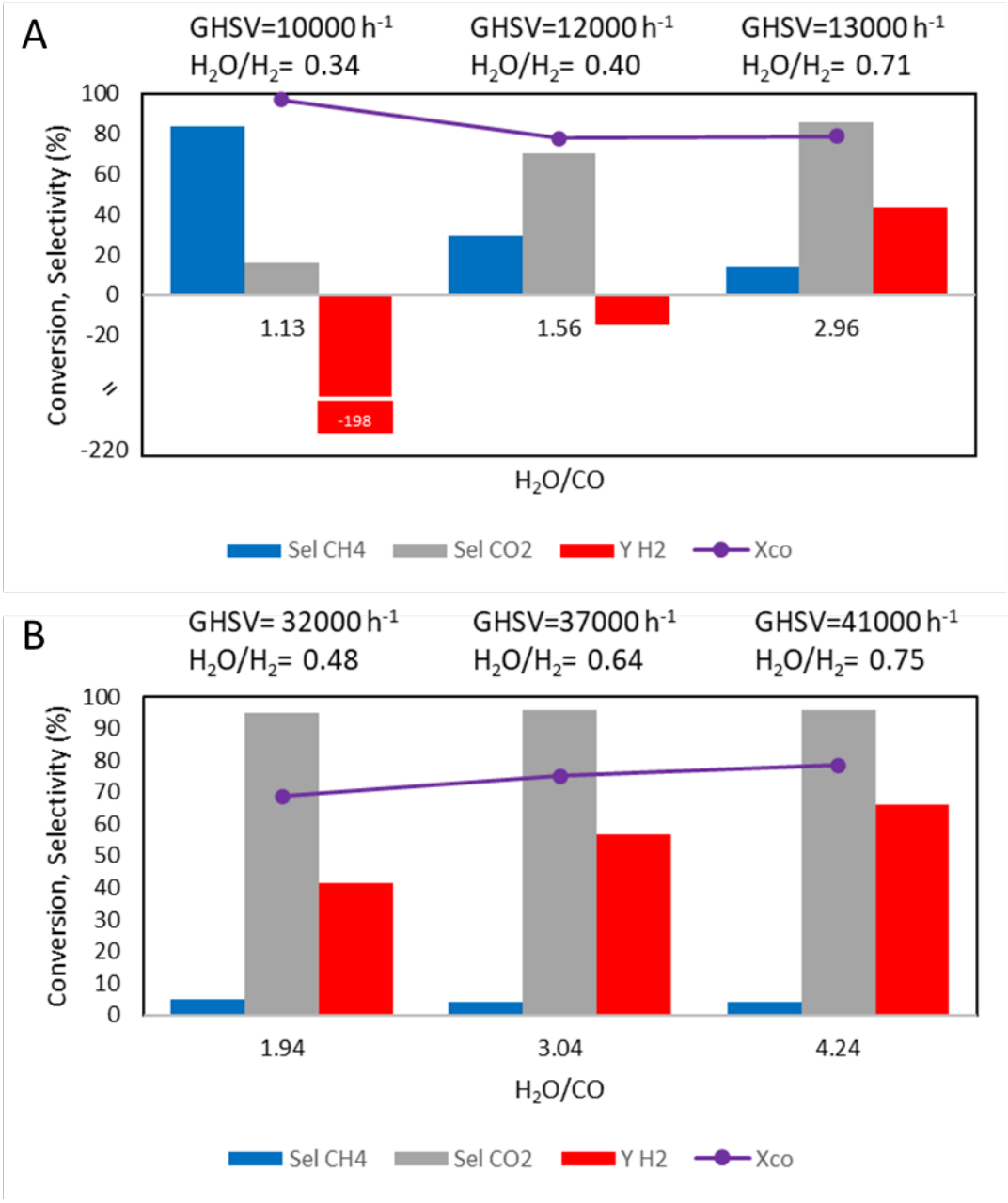

Figure 6: effect of H_2O/CO on CO conversion, methane and carbon dioxide selectivity and hydrogen production on Pt-CZO at low GHSV and 3 atm (A) and high GHSV and 5 atm (B). Equilibrium CO conversion calculated on WGS reaction only. The oxy-reforming reactor was fed with a S/C of 1; 1.5 and 2 respectively resulting in a H_2O/CO of 1.13; 1.56; 1.96 for the tests at low GHSV and 3 atm (A) and in a H_2O/CO of 1,94; 3.04 and 4.24 for the tests at high GHSV and 5 atm (B)

At low values of H_2O/CO (1.13), pressure and GHSV (Figure 6A), a high CO conversion was obtained which decreased with increasing H_2O/CO. This is not consistent with the occurrence of the water gas shift reaction alone. In fact, this reaction should be favoured when the steam

amount is increased as steam is indeed a reagent for the water gas shift reaction. It is thus unexpected to observe a conversion fall at higher H_2O/CO. A better understanding of the whole process can be obtained by looking at the values of methane and carbon dioxide selectivities and reaction rates (Table 4) and hydrogen yield. In fact, at low H_2O/CO (1.13), a negative hydrogen yield, hence a hydrogen consumption, is obtained with high methane rate and low CO_2 one. This can be explained by the occurrence of methanation in place of WGS. Thus, if high contact times (lower GHSV) are employed with low H_2O/CO the methanation reaction is favoured over WGS. However, methanation can be inhibited by increasing the H_2O/CO ratio, as steam is both a reagent of WGS and a product of methanation. This in fact also results in an increase of the inlet H_2O/H_2 ratio, favouring water gas shift over methanation. This is confirmed by the increase of CO_2 selectivity and H_2 yield observed at higher H_2O/CO (and thus H_2O/H_2) showing a hydrogen production rather than consumption at H_2O/CO of 2.96. The observed decrease in CO conversion at higher H_2O/CO can be ascribed not due to a decreased occurrence of WGS but to the inhibition of methanation. At higher GHSV and pressure (5 atm, Figure 6B), methanation occurs to a lower extent even at the lower H_2O/CO 1.94, as shown by the low methane selectivity and reaction rate (Table 4) and the effect of steam on the WGS reaction is evident, with an increase in hydrogen production and CO conversion. It must be noted that here the H_2O/CO and H_2O/H_2 are higher compared to the tests carried out at lower GHSV, as the oxy-reforming S/C was kept constant, and a lower methane and steam conversion at high GHSV resulted in higher H_2O/CO and H_2O/H_2 at the WGS reactor inlet. In general, the obtained results show that the unwanted methanation reaction is favoured at low GHSV (higher contact times) and with low steam concentration. Thus, to favour WGS over methanation the S/C at the reforming inlet was set to 2 and the effect of GHSV was further investigated by performing the reaction at different flow velocities. A S/C of 2 was selected to favour the WGS activity. This led to a lower methane selectivity with an increasing CO conversion and hydrogen production (Figure 7) suggesting that the WGS is a faster reaction than methanation. However, it must be noted that changing the GHSV also resulted in an increased H_2O/CO that contributed to inhibiting methanation.

In general, these results suggest that in a coupled process of oxy-reforming followed by WGS operated in the conditions of the present work it is advisable to feed a higher amount of steam and working at higher GHSV so that WGS is favoured over methanation contributing to hydrogen productivity.

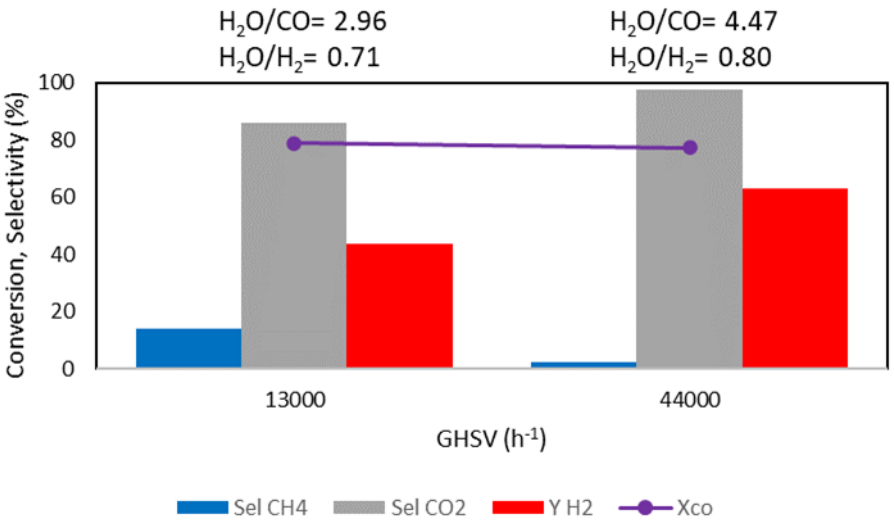

Figure 7: effect of GHSV at 3 atm on CO conversion, methane and carbon dioxide selectivity and hydrogen production on Pt-CZO. Equilibrium CO conversion calculated on WGS reaction only. The oxy-reforming reactor was fed with a S/C of 2.

Finally, the effect of pressure was investigated at low GHSV and high H_2O/CO, obtained by feeding the oxy-reforming with a S/C of 2 (Figure 8). A slight increase in methane selectivity was observed when the pressure was raised from 3 to 5 atm as the methanation reaction produces a decrease in the moles number between reagents and products and is thus favoured at higher pressures. However, hydrogen yield was also increased because of the improved kinetic of the catalyst given by the increase of partial pressures of the reagents. Moreover, the pressure increase also affected the reforming step, lowering the methane and steam conversion and thus increasing the H_2O/CO from 2.96 to 3.80 for the test at 5 atm. This also contributed to favour the WGS reaction leading to higher hydrogen yield.

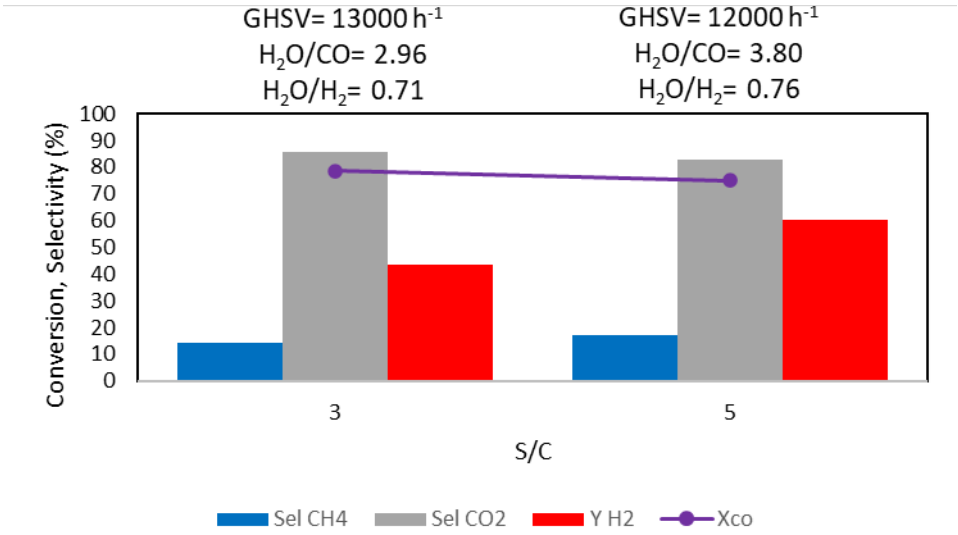

Figure 8: effect of total pressure on CO conversion, methane and carbon dioxide selectivity and hydrogen production on Pt-CZO at 30000 h^{-1} and S/C 2. Equilibrium CO conversion calculated on WGS reaction only. The oxy-reforming reactor was fed with a S/C of 2.

Table 4: water gas shift and methanation reaction rates obtained in the WGS test carried out on Pt-CZO in the fixed bed configuration.

WGS operative conditions	**r_{WGS} ($mol_{CO2}/(s*mol_{Pt})$)**	**$r_{Meth.}$ ($mol_{CO2}/(s*mol_{Pt})$)**
Effect of H_2O/CO (Figure 6A)		
400°C, 10000 h^{-1}, 3 atm, H_2O/CO=1.13	59	307
400°C, 12000 h^{-1}, 3 atm, H_2O/CO=1.56	217	91
400°C, 13000 h^{-1}, 3 atm, H_2O/CO=2.96*	258	43
Effect of H_2O/CO (Figure 6B)		
400°C, 32000 h^{-1}, 5 atm, H_2O/CO=1.94	576	7
400°C, 37000 h^{-1}, 5 atm, H_2O/CO=3.04	663	30
400°C, 41000 h^{-1}, 5 atm, H_2O/CO=4.24	650	28
Effect of GHSV (Figure 7)		
400°C, 13000 h^{-1}, 3 atm, H_2O/CO=2.96 *	258	43
400°C, 44000 h^{-1}, 3 atm, H_2O/CO=4.47	660	16
Effect of pressure (Figure 8)		
400°C, 13000 h^{-1}, 3 atm, H_2O/CO=2.96 *	258	43
400°C, 12000 h^{-1}, 5 atm, H_2O/CO=3.80	208	43

The catalytic tests carried out in the fixed bed WGS reactor showed how, the occurrence of methanation can be detrimental, especially in certain conditions (low GHSV and low H_2O/CO). In light of the obtained results and in order to get further insights into the role that the membrane reactor can have on the WGS and methanation selectivity, it is important to discuss the reaction mechanism involved in these catalytic processes. In particular, when a reformate mixture is further converted with the aim of hydrogen production three main reactions can occur: the desired water gas shift reaction and the undesired CO and CO_2 methanation. The water gas shift reaction mechanism depends not only on the reaction conditions but also on the type of catalyst employed and different pathways have been proposed [51–56]. For Pt/CeO_2 catalysts two main pathways are considered for WGS called the redox and associative mechanisms [51,57–59]. During the redox mechanism CO adsorption occurs on the surface of Pt, followed by its diffusion toward the metal-support interface, where it reacts with the mobile O of the cerium oxide to give CO_2. The reduced Ce^{3+} site is then regenerated by steam dissociation, which also contributes to H_2 formation. In the associative mechanism, water dissociation on the support leads to the formation of -OH groups that leads to the formation of a formate reaction intermediate after reaction with CO adsorbed on Pt [51]. Kalamaras et al. actually showed by steady-state isotopic transient kinetic analysis and transient isotopic experiments that the actual mechanism is a combination of the two, where CO adsorbed on Pt leads to the formation of a formate intermediate with the labile oxygen of the cerium oxide. This formate transforms then in carbon dioxide leaving an oxygen vacancy over the support that is re-oxidized by steam, leading also to H_2 production [51]. In all cases the active site for CO association is given by Pt surface while water interacts with the support.

Carbon monoxide methanation is as well described by two mechanisms that involve the CO adsorption on metal surface, namely the associative and dissociative mechanisms [60]. The former regards the hydrogenation of adsorbed CO by adsorbed H (H_{ads}) obtained by hydrogen dissociative chemisorption occurring on the metal surface as well. The latter involves the dissociative chemisorption of CO to adsorbed C and O followed by their hydrogenation by H_{ads} [61]. In this case both reagents, i.e. CO and H_2, are dissociated on metallic sites.

Finally, CO_2 methanation have been reported to undergo two possible mechanisms, dependent on the employed catalyst, and they are again called associative or dissociative mechanism [62–67]. In associative one, carbon dioxide adsorbs on the support as a formate and reacts with H_{ads} that has been chemisorbed over the metallic surface and reaches the metal support interface by spillover. After different hydrogenation steps methane is produced. On the other hand, CO_2

produces an adsorbed carbonyl intermediate in the dissociative route from dissociation over the metal. The carbonyl then reacts with H_{ads} to give methane. The main difference between the two mechanisms is that support sites participate to the associative mechanisms. As already recalled the mechanism involved depends strongly on the catalysts and different authors have shown that the associative one is the preferred pathway on metal supported CeZr oxides due to the contribution of the support in formate formation [68,69].

Summing up the consideration made over the mechanisms involved the main differences between the three reactions regard the active sites and the co-reagent for CO conversion. WGS requires H_2O as co-reagent, metal active sites for CO adsorption and support sites for H_2O conversion; CO methanation occurs over the metal for both CO and hydrogen adsorption, the latter acting as co-reagent. Methanation involved the adsorption of hydrogen co-reagent as well over the metal, while CO_2 interacts with the support. Thus, the extent of the reactions is driven by the availability of the active sites which is also dependent on the relative concentration of the reagents. In fact, high steam concentrations provide a high reoxidation of the reduced ceria sites favouring CO oxidation to CO_2 and hydrogen production. On the opposite high hydrogen concertation would saturate the metal sites, competing with CO adsorption or favouring its reduction leading to methane formation. This is confirmed by the values of the relative concentration of steam and hydrogen reported in Figures 6, 7 and 8, which shows how methane selectivity is decreased at high H_2O/H_2 ratios. When the H_2O/H_2 increases from 0.34 to 0.40 and then 0.71 due to a raise in the H_2O/CO inlet (Figure 6A), a sudden drop in methane selectivity was observed as the presence of a more oxidative environment and of higher concentrations of water favoured the reoxidation of ceria by the latter, supporting the WGS reaction mechanism [51]. The $Ce_{0.5}Zr_{0.5}O_2$ support indeed plays a crucial role in supporting the WGS mechanism by providing oxygen to the adsorbed CO thanks to its oxygen storage and oxygen release properties. These are well known properties for these kind of systems and the formation of $Ce_{0.5}Zr_{0.5}O_2$ nanospheres templated through the microemulsion synthesis, as carried out in this work, increased the oxygen storage compared to other synthetic methods [25]. The H_2O/H_2 also raised at higher GHSV, showing again higher selectivity for the WGS reaction, while an increase in total pressure had slight effect on the occurrence of the latter and methanation.

This implies that high ratio of steam should be used, which however can be expensive in terms of reactor volume and heat of evaporation, while the use of streams already containing high hydrogen concentrations coming from reforming may lead to unwanted methane formation. In

general, the hydrogen concentration in the reaction environment is crucial to discriminate between WGS and methanation, with high hydrogen concentrations favouring the latter. Another way to increase the H_2O/H_2 would be to reduce the concentration of hydrogen. To further investigate this concept and to provide a method for the in-situ removal of hydrogen from the catalyst without affecting its productivity, the WGS tests were carried out inside a Pd membrane, in the membrane reactor configuration.

3.4. WGS reaction in a membrane reactor

After investigating the water gas shift process in a fixed bed reactor, the attention of this study focused on the membrane reactor setup, where the former process is carried out inside the tubular thin Pd/TS-1 membrane with the aim of producing pure hydrogen already in the WGS step and understanding the effect of H_2 removal from the reaction environment on the overall process. With this purpose, the results obtained over Pt-CZO placed inside the membrane and fed with the oxy-reforming outlet, where compared with those obtained in the same conditions in the fixed bed WGS. The TS-1 porous protective layer was used to avoid direct contact between the catalyst and the Pd, which may lead to the deactivation of the membrane.

At first conditions where WGS was favoured over methanation and in which Pt-CZO proved to be able to increase hydrogen production in fixed bed were selected. Figure 9 compares hydrogen yield and CO conversion obtained on Pt-CZO in the fixed bed and in the membrane reactor configuration.

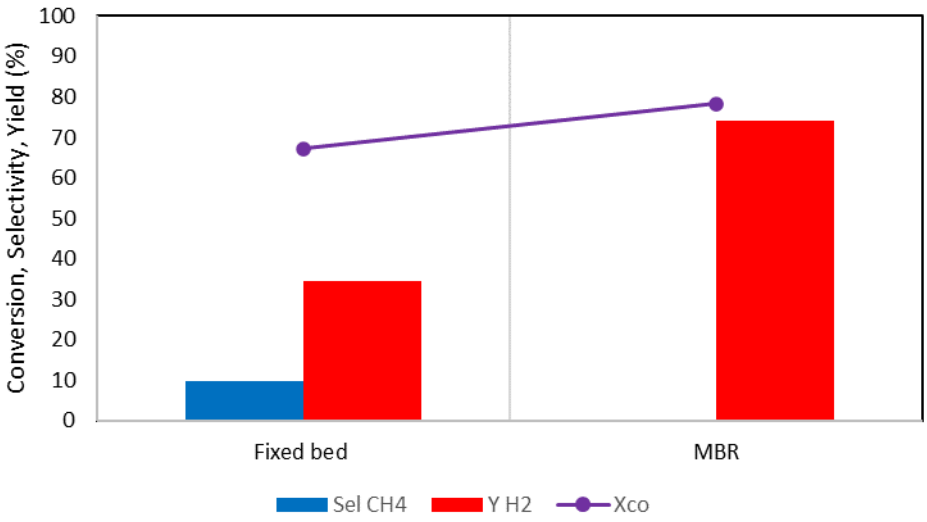

Figure 9: CO conversion, hydrogen yield and methane selectivity obtained in the fixed bed or membrane reactor charged with Pt-CZO and fed with the outlet of the oxy-reforming reactor which was run at 32000 h^{-1}, 3 atm and $H_2O/CO=1.68$.

Under these conditions, Pt-CZO was able to provide a high CO conversion of 68% in fixed bed as previously discussed. Hydrogen yield was 35% and was held back by the occurrence of methanation as highlighted by the production of methane and concurrent hydrogen consumption. In the case of water gas shift membrane reactor, most of the produced hydrogen was directly separated thought the thin Pd layer that composes the walls of the reactor, and this phenomenon influenced the whole catalytic process. A further discussion on the efficiency of the separation will be presented in the next chapter, while here we would like to focus on the effect that the membrane reactor configuration provides, where hydrogen production and separation occur in the same environment. Under the membrane reactor configuration, the reagents are sent in the inner side of the Pd-based membrane, where the catalyst is also placed. The hydrogen already produced in the oxy-reforming step, as well as those produced over the Pt-based catalyst, spread toward the membrane walls, and diffuses toward the Pd dense layer, being removed by the reaction environment and creating a dynamic equilibrium when the hydrogen that is produced is readily sequestrated and purified supporting the conversion of carbon monoxide. When the reaction was run in the membrane reactor, H_2 yield and CO conversion raised to 73% and 90% respectively, while methane selectivity dropped with no methane production in the membrane reactor. In fact, hydrogen purification avoided its consumption to CH_4, locally increasing the H_2O/H_2 ratio and favouring the WGS mechanism over methanation. Interestingly, the CO conversion was higher than the equilibrium

conversion expected for a fixed bed reactor, because of the hydrogen removal that created a dynamic equilibrium that pushed toward further hydrogen production and CO conversion.

A similar behaviour was observed at higher pressure (5 atm) and H_2O/CO, where again hydrogen yield was increased by 20% and CO conversion by 15%, with no methane produced in the presence of the membrane (Figure 10).

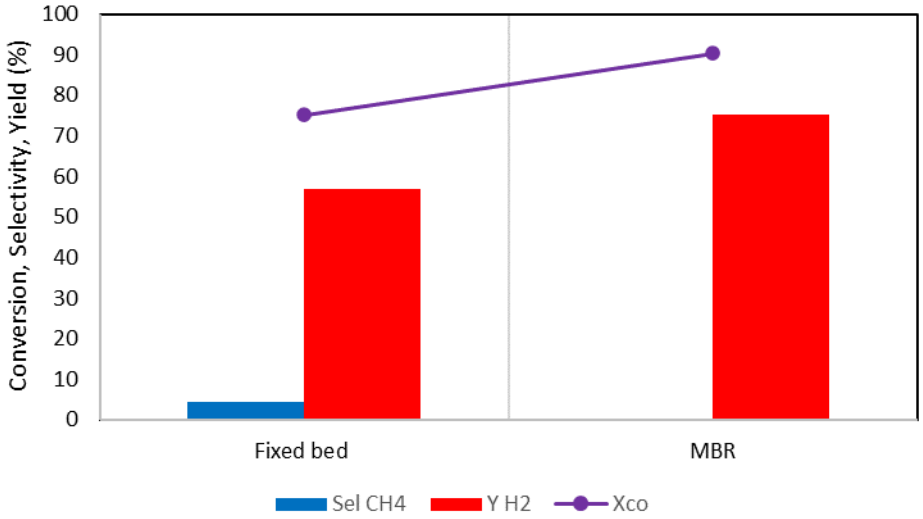

Figure 10: CO conversion, hydrogen yield and methane selectivity obtained in the fixed bed or membrane reactor charged with Pt-CZO and fed with the outlet of the oxy-reforming reactor which was run at 37000 h^{-1}, 3 atm and H_2O/CO=3.04

However, the most interesting results were obtained at lower GHSV, conditions where the methanation reaction was favoured over the WGS one in the fixed bed configuration and led to hydrogen consumption (Figure 11). 10000 h^{-1}, 3 atm, H_2O/CO =1.13 (Figure 11A) total CO conversion was observed in the fixed bed, which however was caused by the production of methane, as previously discussed and reported in Figure 6. Interestingly, the fast hydrogen separation obtained with the thin Pd-membrane characterized by high permeance, avoided the occurrence of the hydrogen consuming reactions, removing the hydrogen reagent and increasing the H_2O/H_2 ratio, promoting WGS and suppressing methanation. At higher H_2O/CO the fixed bed provided methanation to a lower extent as previously discussed. Nevertheless, hydrogen was still consumed rather than produced under these conditions. On the opposite high hydrogen yields and CO conversion were obtained with the membrane reactor, that were even higher that at lower H_2O/CO as the addition of further steam boosted the WGS activity. The results presented here clearly shows how the increased hydrogen production obtained in these tests are not only caused by the increase of the water gas shift

reaction by the creation of a dynamic equilibrium thanks to the Le Chatelier's principle, but also to the suppression of methane formation reaction mechanism. In fact, the removal of hydrogen and the resulting increase of H_2O/H_2 ratio led to a high reoxidation rate of ceria sites by steam that allowed fast CO oxidation to CO_2 and concurrent hydrogen production.

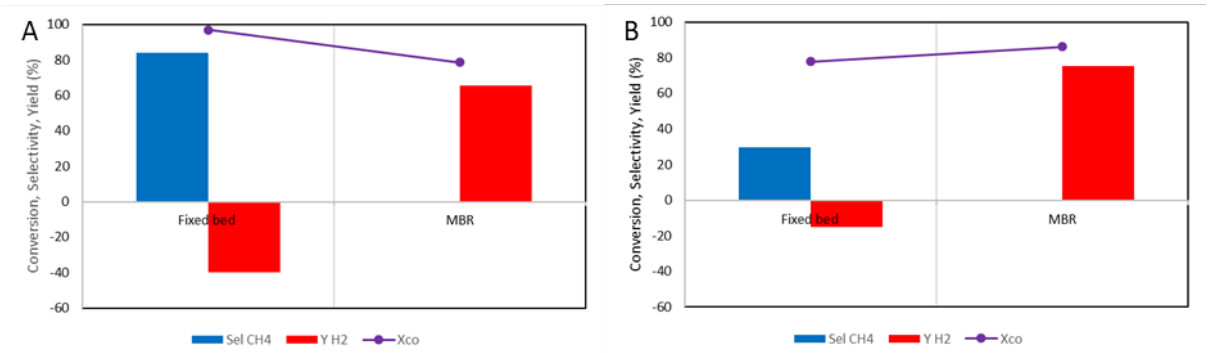

Figure 11: CO conversion, hydrogen yield and methane selectivity obtained in the fixed bed or membrane reactor charged with Pt-CZO and fed with the outlet of the oxy-reforming reactor which was run at (A) 10000 h^{-1}, 3 atm, H_2O/CO =1.13 and (B) 120000 h^{-1}, 3 atm, H_2O/CO =1.56

Having understood the mechanism occurring in membrane reactors and how it favours hydrogen yield, the operative conditions of the MBR were optimized with the aim of maximizing productivity and hydrogen recovery in the purified stream.

3.5. Maximization of H_2 recovery and pure stream

The reaction conditions of the combined oxy-reforming and WGS process were optimized with the aim of maximizing the pure hydrogen flux and the hydrogen recovery, coupled with the high CO conversions and hydrogen yield shown in the previous chapter.

To better understand how the operative conditions influence the separation phenomenon, it is important to have a look at the formula governing hydrogen permeation through Pd-based membranes, i.e., the Sievert-Fick equation:

$$JH2 = \frac{Pe_{H2}(p^n{}_{H2}, \text{ret} - p^n{}_{H2}, \text{perm})}{\delta}$$

Where J_{H2} is the hydrogen flux through the membrane, Pe_{H2} is the permeability of hydrogen, $p^n{}_{H2}$,ret and $p^n{}_{H2}$,perm are the partial pressures of hydrogen at the retentate (where WGS occurs) and permeate side (where hydrogen is separated) respectively and δ is the thickness of the palladium layer. Finally, n is a constant that depends on the type of membrane, and it is 0.7 in the case of this study as reported in the experimental. Analysing the Sievert-Fick equation

some useful considerations can be drawn and help to identify the best reaction conditions for the membrane reactor. To have a high permeated flux three parameters can be optimized: (i) permeability; (ii) membrane thickness and (iii) difference in hydrogen partial pressure between retentate and permeate side. Here, the Pd-based membrane was obtained by electroless plating deposition over a porous alumina tube, which allowed to give high permeability, thanks to Pd properties, and the thin Pd layer (2 microns) [37]. These parameters are set in the membrane production step and for this reason, the only parameter that can be operatively tuned is the hydrogen partial pressure. The use of the Pt-CZO catalyst inside the membrane reactor allowed to increase hydrogen partial pressure by its production by WGS. Moreover, hydrogen partial pressure can be increased by raising total pressure of the combined oxy-reforming-WGS system.

Total pressure was found to be a key parameter to increase purified hydrogen flux and hydrogen recovery. Table 5 reports the results obtained at high GHSV and different pressures (3, 5 and 10 atm) for the oxy-reforming followed by WGS membrane reactor. To further enhance hydrogen recovery, in the case of the test at 10 atm, the oven temperature of the oxy-reforming reactor was raised from 750 to 840°C, to increase methane conversion and hydrogen production in the first step.

Table 5: Hydrogen recovery and permeated hydrogen flux obtained in the integrated oxy-reforming and WGS carried out in a membrane reactor at different pressures.

Oxy-reforming operative conditions 750°C, S/C=1.50 O/C=0.21, 100000 h^{-1}	**H_2 partial pressure retentate inlet (atm)**	**H_2 partial pressure permeate (atm)**	**Permeate H_2 flux (ml/min)**	**Hydrogen recovery (%)**
3 atm, 37000 h^{-1}	1.2	1.0	175	29
5 atm, 37000 h^{-1}	2.0	1.0	315	51
10 atm, 38000 h^{-1} (oxy-ref at 840°C)	4.9	1.0	685	89

Increasing total pressure from 3 to 5 and then to 10 bars led to a consistent increase in hydrogen recovery, from 39% to 51% and 89% with a concurrent increase of the pure hydrogen flux from

182 ml/min to 315 ml/min and 731 ml/min. This increase was caused by the raising driving force given by the higher hydrogen partial pressure at the membrane inlet for the tests at 5 and 10 bar, which favoured hydrogen separation. In the case of the test at 10 atm, the membrane inlet H_2 partial pressure was 4.5 atm, while a hydrogen partial pressure of 1.3 was measured at the membrane outlet. Thus still a small driving force of Δp of 0.3 atm between retentate and permeate (which is kept at 1 atm) was observed. This indicated that the membrane has been fully exploited, differently from what happened for the empty membrane, thanks to the in-situ hydrogen production by WGS that helped to increase hydrogen partial pressure, hence the separation driving force. This resulted in 89% hydrogen recovery, which indicates that almost all the produced hydrogen has been purified. This value places among the highest in the literature for Pd-based WGS membrane reactors (Table 6). A comprehensive comparison of the literature results is made difficult by the different operative conditions, catalysts and membranes reported. In particular, there is a lack of uniformity in the maximum total pressure used, which however, highly influences the permeation of hydrogen as it raises the separation driving force (H_2 partial pressure). For this reason, the comparison between the hydrogen recoveries must be accompanied by a rationalization of the reaction conditions. For instance, high recovery (83%) was reported also at low pressure and temperature (1 atm, 325°C) [24]. The same value was disclosed by other authors under harsher conditions (11 atm, 395°C) [19], while the highest values of 88% and 90% were respectively shown at 450°C and 8 atm [20] or 14 atm [22]. However, the results of this work provide some advancements with respect to the literature. In fact, although different reaction conditions and systems have been reported, most of the reported works carried out the water gas shift reaction in the membrane by employing simulated WGS feeds, while an integration with the upstream reforming process is reported here. In addition, the process studied in this work was carried out at higher GHSV compared to other works, a parameter that is fundamental for high hydrogen productivities and that may decrease the separation efficiency. Finally, the high hydrogen recovery (89%) was obtained without using a sweep gas. Although the employment of a sweep gas increases hydrogen permeation by decreasing the hydrogen partial pressure at the retentate side, diluting the separated hydrogen, it also adds a cost to the process. Laboratory experiments are usually carried out employing nitrogen as a sweep gas for matters of simplicity. However, to recover the separated hydrogen in a pure form, easily separable gases such as steam should be used, which however require considerable costs for their vaporization. On the opposite, the absence of sweep gas in thin Pd membranes has been reported to result in concentration polarization effect that decreases the permeated hydrogen flux due to the formation of a thin film of non-

permeating gases in proximity of the membrane layer. However, the hydrogen permeated fluxes are proportional to the employed pressure (hence to the driving force of the permeation through the dense layer), indicating that this phenomenon is avoided here (Figure 12). This is due to high total fluxes employed in this work compared to literature (Table 6) that create a turbulent regime which avoids the formation of stagnant films even in the absence of a sweep gas.

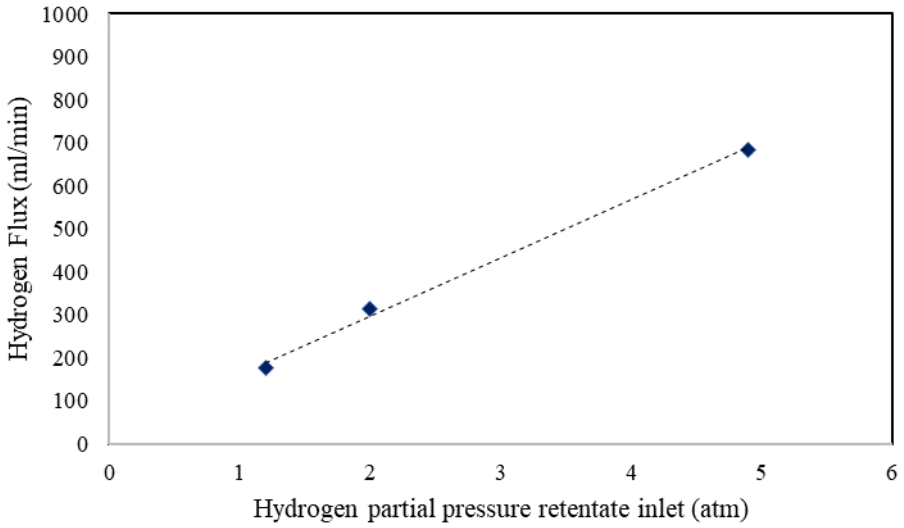

Figure 12: Hydrogen permeated fluxes obtained in the integrated oxy-reforming and WGS carried out in a membrane reactor as a function of hydrogen partial pressure inside the membrane.

Table 6: Hydrogen recoveries obtained in state-of-the-art Pd-based water gas shift membrane reactors.

Membrane	**Feed Gas**	**T (°C)**	**P (atm)**	**GSHV (h^{-1})**	**Sweep gas**	**H_2 recovery**	**Ref**
Pd-Ag	H_2O/ CO	325	1	$1.95x10^{-5}$*	Yes	83%	[24]
Pd77%-Ag23%	H_2O/ CO/CO_2	430	4	Not reported	No	82%	[17]
Pd	H_2O/ CO/N_2	450	3	840**	Yes	16%	[18]
Pd77%-Ag23%	H_2O/ CO	450	8	6240	Yes	90%	[20]
Pd	H_2/H_2O/ CO/CO_2	450	14.4	2000	No	88%	[22]
Pd	H_2O/ CO	390	11	3450	No	83%	[19]

Pd-Ag	H_2O/ CO/He	500	2.5	5793	Yes	65%	[23]
Pd-Au-Pd	Reforming +WGS in the MBR	450	5	600	No	45%	[21]
Pd	**From oxy-reforming**	**400**	**10**	**38000**	**No**	**89%**	**This work**

** mol CO/s; **L/h*g_{cat}*

3.6. Characterization of the used catalyst

Carbon formation over the catalyst or membrane is a side-reaction that can occur in the presence of methane and carbon monoxide especially, if low amount of steam and hydrogen are present, as is the case of the membrane reactor operation where hydrogen is readily removed by the reaction environment [70,71]. Thus, the used catalyst and membrane were analysed by Raman analysis to probe the eventual presence of carbon deposits that may have led to deactivation. Carbon can be identified by Raman analysis as it displays two main bands around 1350 and 1550 cm^{-1} [72]. The analysis of the catalyst evidenced the absence of carbon deposits (Figure 13), which was thanks to the oxygen storage capacity and oxygen mobility properties of the Ce based support that are known to provide oxygen to the eventually formed carbon, removing it from the catalyst surface [25,42].

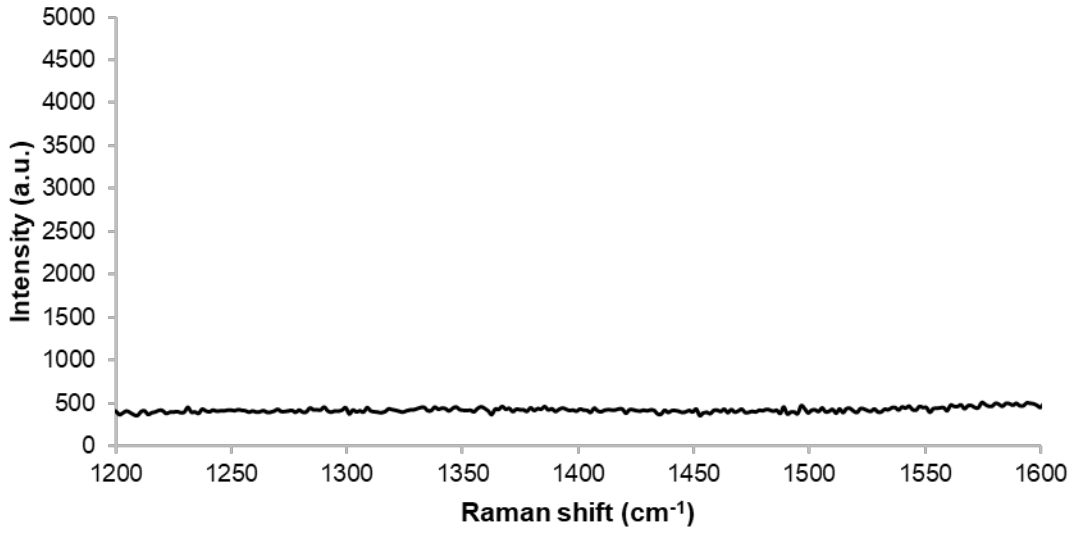

Figure 13: Raman analysis of the Pt-CZO catalyst after the WGS membrane reactor tests.

4. Conclusions

The present study reports the synthesis of Rh and Pt supported over $Ce_{0.5}Zr_{0.5}O_2$ obtained by microemulsion and applied to the methane oxy-reforming and water gas shift integrated processes with the aim of pure hydrogen production. To fulfil so, it investigated the use of Pd-based membranes, which are selectively permeable toward H_2. At first, an empty membrane at 400°C was placed after the oxy-reforming conducted at 750°C giving a pure hydrogen flux. However, the driving force of permeation was not fully exploited and for this reason the membrane was loaded with the $Pt/Ce_{0.5}Zr_{0.5}O_2$ catalyst to perform the water gas shift reaction on the produced reformate mixture. To get insights in the effect provided by the membrane a WGS fixed bed configuration was compared to the membrane reactor one. In the first case, the occurrence of the methanation reaction was observed, consuming hydrogen, and was related to the operative conditions and mainly addressed to high H_2/H_2O ratios in the feed, that favoured the methanation mechanism over the WGS one. The use of the membrane reactor allowed to remove the produced hydrogen, increasing the CO conversion over the equilibrium value of the fixed bed, increasing hydrogen yield for the Le Chatelier's principle and avoiding methane formation by locally decreasing the H_2/H_2O ratio, even when this value was high at the membrane inlet. Optimization of the operative conditions of the integrated processes allowed to obtain a pure hydrogen flux from methane in just two steps with anhigh hydrogen recovery of 89% without using any sweep gas.

Funding

This research did not receive any specific grant from funding agencies in the public, commercial, or not-for-profit sectors.

5. Credit author statement

Andrea Fasolini: Methodology, Validation, Investigation, Data curation, Visualization, Writing - Original Draft, Writing - Review & Editing **Rodolfo Mafessanti:** Methodology, Validation, Investigation, Data curation **Salvatore Abate:** Conceptualization, Methodology, Validation, Investigation, Writing - Review & Editing **Pio Gramazio:** Investigation, Data curation, Writing - Review & Editing **Jacopo De Maron:** Data curation**,** Writing - Review & Editing **Gabriele Centi:** Conceptualization, Resources, Writing - Review & Editing, Funding acquisition, Supervision, Project administration **Francesco Basile:** Conceptualization, Resources, Writing - Review & Editing, Funding acquisition, Supervision, Project administration

6. References

[1] L. Barreto, A. Makihira, K. Riahi, The hydrogen economy in the 21st century: a sustainable development scenario, Int. J. Hydrog. Energy. 28 (2003) 267–284. https://doi.org/10.1016/S0360-3199(02)00074-5.

[2] N.P. Brandon, Z. Kurban, Clean energy and the hydrogen economy, Philos. Trans. R. Soc. Math. Phys. Eng. Sci. 375 (2017) 20160400. https://doi.org/10.1098/rsta.2016.0400.

[3] J.O. Abe, A.P.I. Popoola, E. Ajenifuja, O.M. Popoola, Hydrogen energy, economy and storage: Review and recommendation, Int. J. Hydrog. Energy. 44 (2019) 15072–15086. https://doi.org/10.1016/j.ijhydene.2019.04.068.

[4] Communication COM/2020/301: A hydrogen strategy for a climate-neutral Europe | Knowledge for policy, (n.d.). https://knowledge4policy.ec.europa.eu/publication/communication-com2020301-hydrogen-strategy-climate-neutral-europe_en (accessed April 27, 2021).

[5] L. Cornaglia, J. Múnera, E. Lombardo, Recent advances in catalysts, palladium alloys and high temperature WGS membrane reactors: A review, Int. J. Hydrog. Energy. 40 (2015) 3423–3437. https://doi.org/10.1016/j.ijhydene.2014.10.091.

[6] E. Meloni, M. Martino, V. Palma, A Short Review on Ni Based Catalysts and Related Engineering Issues for Methane Steam Reforming, Catalysts. 10 (2020) 352. https://doi.org/10.3390/catal10030352.

[7] M.V. Twygg, Catalyst Handbook, 2 edition, Oxford University Press, London, 1997.

[8] G.A. de Queiroz, C.M.B. de Menezes Barbosa, C. A. Pimentel, C.A.M. de Abreu, Performance of the water gas shift process with a ruthenium catalyst for hydrogen production in a membrane reactor, React. Kinet. Mech. Catal. 123 (2018) 679–687. https://doi.org/10.1007/s11144-017-1313-9.

[9] S. SIRCAR, T.C. GOLDEN, Purification of Hydrogen by Pressure Swing Adsorption, Sep. Sci. Technol. 35 (2000) 667–687. https://doi.org/10.1081/SS-100100183.

[10] G. Iaquaniello, E. Palo, A. Salladini, Pd-Based Membrane Reactors for Syngas Preparation and WGS, in: Membr. React. Eng., John Wiley & Sons, Ltd, 2016: pp. 184–200. https://doi.org/10.1002/9781118906842.ch9.

[11] D. Capoferri, B. Cucchiella, G. Iaquaniello, A. Mangiapane, S. Abate, G. Centi, Catalytic Partial Oxidation and Membrane Separation to Optimize the Conversion of Natural Gas to Syngas and Hydrogen, ChemSusChem. 4 (2011) 1787–1795. https://doi.org/10.1002/cssc.201100260.

[12] A. Basile, G. Chiappetta, S. Tosti, V. Violante, Experimental and simulation of both Pd and Pd/Ag for a water gas shift membrane reactor, Sep. Purif. Technol. 25 (2001) 549–571. https://doi.org/10.1016/S1383-5866(01)00168-X.

[13] M.R. Rahimpour, F. Samimi, A. Babapoor, T. Tohidian, S. Mohebi, Palladium membranes applications in reaction systems for hydrogen separation and purification: A review, Chem. Eng. Process. Process Intensif. 121 (2017) 24–49. https://doi.org/10.1016/j.cep.2017.07.021.

[14] D. Mendes, A. Mendes, L.M. Madeira, A. Iulianelli, J.M. Sousa, A. Basile, The water-gas shift reaction: from conventional catalytic systems to Pd-based membrane reactors—a review, Asia-Pac. J. Chem. Eng. 5 (2010) 111–137. https://doi.org/10.1002/apj.364.

[15] W. Gao, T. Zhou, Y. Gao, Q. Wang, Enhanced water gas shift processes for carbon dioxide capture and hydrogen production, Appl. Energy. 254 (2019) 113700. https://doi.org/10.1016/j.apenergy.2019.113700.

[16] A. Basile, A. Criscuoli, F. Santella, E. Drioli, Membrane reactor for water gas shift reaction, Gas Sep. Purif. 10 (1996) 243–254. https://doi.org/10.1016/S0950-4214(96)00024-2.

[17] L.N. Baloyi, B.C. North, H.W. Langmi, B.J. Bladergroen, T.V. Ojumu, The production of hydrogen through the use of a 77 wt% Pd 23 wt% Ag membrane water gas shift reactor, South Afr. J. Chem. Eng. 22 (2016) 44–54. https://doi.org/10.1016/j.sajce.2016.11.001.
[18] S. Jamshidi, A. Noruzi, A.A. Babaluo, M. Haghighi, Performance of Pd composite membrane prepared by organic–inorganic method in WGS membrane reactor, Sep. Sci. Technol. 51 (2016) 1891–1899. https://doi.org/10.1080/01496395.2016.1186188.
[19] S. Liguori, P. Pinacci, P.K. Seelam, R. Keiski, F. Drago, V. Calabrò, A. Basile, A. Iulianelli, Performance of a Pd/PSS membrane reactor to produce high purity hydrogen via WGS reaction, Catal. Today. 193 (2012) 87–94. https://doi.org/10.1016/j.cattod.2012.02.005.
[20] C.A. Cornaglia, S. Tosti, M. Sansovini, J. Múnera, E.A. Lombardo, Novel catalyst for the WGS reaction in a Pd-membrane reactor, Appl. Catal. Gen. 462–463 (2013) 278–286. https://doi.org/10.1016/j.apcata.2013.04.019.
[21] B. Castro-Dominguez, I. Mardilovich, L.-C. Ma, R. Ma, A. Dixon, N. Kazantzis, Y. Ma, Integration of Methane Steam Reforming and Water Gas Shift Reaction in a Pd/Au/Pd-Based Catalytic Membrane Reactor for Process Intensification, Membranes. 6 (2016) 44. https://doi.org/10.3390/membranes6030044.
[22] A.S. Augustine, Y.H. Ma, N.K. Kazantzis, High pressure palladium membrane reactor for the high temperature water–gas shift reaction, Int. J. Hydrog. Energy. 36 (2011) 5350–5360. https://doi.org/10.1016/j.ijhydene.2011.01.172.
[23] S. Pati, A. Jangam, Z. Wang, N. Dewangan, M.H. Wai, S. Kawi, Catalytic Pd0.77Ag0.23 alloy membrane reactor for high temperature water-gas shift reaction: Methane suppression, Chem. Eng. J. 362 (2019) 116–125. https://doi.org/10.1016/j.cej.2018.12.112.
[24] S. Tosti, A. Basile, G. Chiappetta, C. Rizzello, V. Violante, Pd–Ag membrane reactors for water gas shift reaction, Chem. Eng. J. 93 (2003) 23–30. https://doi.org/10.1016/S1385-8947(02)00113-4.
[25] F. Basile, R. Mafessanti, A. Fasolini, G. Fornasari, E. Lombardi, A. Vaccari, Effect of synthetic method on CeZr support and catalytic activity of related Rh catalyst in the oxidative reforming reaction, J. Eur. Ceram. Soc. 39 (2019) 41–52. https://doi.org/10.1016/j.jeurceramsoc.2018.01.047.
[26] A. Gondolini, A. Fasolini, E. Mercadelli, F. Basile, A. Sanson, Freeze cast porous membrane catalyst for hydrogen production via oxy-reforming, Fuel Process. Technol. 213 (2021) 106658. https://doi.org/10.1016/j.fuproc.2020.106658.
[27] A. Fasolini, S. Abate, D. Barbera, G. Centi, F. Basile, Pure H2 production by methane oxy-reforming over Rh-Mg-Al hydrotalcite-derived catalysts coupled with a Pd membrane, Appl. Catal. Gen. 581 (2019) 91–102.
[28] C. Hognon, Y. Simon, P.-M. Marquaire, C. Courson, A. Kiennemann, Hydrogen production by catalytic partial oxidation of propane over CeO2, Chem. Eng. Sci. 181 (2018) 46–57. https://doi.org/10.1016/j.ces.2018.01.038.
[29] C. Lang, X. Sécordel, A. Kiennemann, C. Courson, Water gas shift catalysts for hydrogen production from biomass steam gasification, Fuel Process. Technol. 156 (2017) 246–252. https://doi.org/10.1016/j.fuproc.2016.09.004.
[30] A. Auxéméry, B.B. Frias, E. Smal, K. Dziadek, G. Philippot, P. Legutko, M. Simonov, S. Thomas, A. Adamski, V. Sadykov, K. Parkhomenko, A.-C. Roger, C. Aymonier, Continuous supercritical solvothermal preparation of nanostructured ceria-zirconia as supports for dry methane reforming catalysts, J. Supercrit. Fluids. 162 (2020) 104855. https://doi.org/10.1016/j.supflu.2020.104855.
[31] L. Jurado, N. García-Moncada, L.F. Bobadilla, F. Romero-Sarria, J.A. Odriozola, Elucidation of Water Promoter Effect of Proton Conductor in WGS Reaction over Pt-Based Catalyst: An Operando DRIFTS Study, Catalysts. 10 (2020) 841. https://doi.org/10.3390/catal10080841.

[32] W.N. Manan, W.N.R. Wan Isahak, Z. Yaakob, CeO2-Based Heterogeneous Catalysts in Dry Reforming Methane and Steam Reforming Methane: A Short Review, Catalysts. 12 (2022) 452. https://doi.org/10.3390/catal12050452.
[33] T. Montini, M. Melchionna, M. Monai, P. Fornasiero, Fundamentals and Catalytic Applications of CeO2-Based Materials, Chem. Rev. 116 (2016) 5987–6041. https://doi.org/10.1021/acs.chemrev.5b00603.
[34] Y. Bi, H. Xu, W. Li, A. Goldbach, Water–gas shift reaction in a Pd membrane reactor over Pt/Ce0.6Zr0.4O2 catalyst, Int. J. Hydrog. Energy. 34 (2009) 2965–2971. https://doi.org/10.1016/j.ijhydene.2009.01.046.
[35] A. Fasolini, S. Ruggieri, C. Femoni, F. Basile, Highly Active Catalysts Based on the Rh4(CO)12 Cluster Supported on Ce0.5Zr0.5 and Zr Oxides for Low-Temperature Methane Steam Reforming, Catalysts. 9 (2019) 800. https://doi.org/10.3390/catal9100800.
[36] S. Abate, C. Genovese, S. Perathoner, G. Centi, Performances and stability of a Pd-based supported thin film membrane prepared by EPD with a novel seeding procedure. Part 1—Behaviour in H2: N2 mixtures, Catal. Today. 145 (2009) 63–71.
[37] S. Abate, U. Díaz, A. Prieto, S. Gentiluomo, M. Palomino, S. Perathoner, A. Corma, G. Centi, Influence of Zeolite Protective Overlayer on the Performances of Pd Thin Film Membrane on Tubular Asymmetric Alumina Supports, Ind. Eng. Chem. Res. 55 (2016) 4948–4959. https://doi.org/10.1021/acs.iecr.6b00690.
[38] S. Abate, G. Giorgianni, S. Gentiluomo, G. Centi, S. Perathoner, Enhanced Hydrogen Transport over Palladium Ultrathin Films through Surface Nanostructure Engineering, ChemSusChem. 8 (2015) 3805–3814.
[39] A. Fasolini, E. Lombardi, T. Tabanelli, F. Basile, Microemulsion Derived Titania Nanospheres: An Improved Pt Supported Catalyst for Glycerol Aqueous Phase Reforming, Nanomaterials. 11 (2021) 1175. https://doi.org/10.3390/nano11051175.
[40] V. Maslova, A. Fasolini, M. Offidani, S. Albonetti, F. Basile, Solar-driven valorization of glycerol towards production of chemicals and hydrogen, Catal. Today. 380 (2021) 147–155. https://doi.org/10.1016/j.cattod.2021.03.008.
[41] V. Maslova, E.A. Quadrelli, P. Gaval, A. Fasolini, S. Albonetti, F. Basile, Highly-dispersed ultrafine Pt nanoparticles on microemulsion-mediated TiO2 for production of hydrogen and valuable chemicals via oxidative photo-dehydrogenation of glycerol, J. Environ. Chem. Eng. 9 (2021) 105070. https://doi.org/10.1016/j.jece.2021.105070.
[42] J. De Maron, R. Mafessanti, P. Gramazio, E. Orfei, A. Fasolini, F. Basile, H2 Production by Methane Oxy-Reforming: Effect of Catalyst Pretreatment on the Properties and Activity of Rh-Ce0.5Zr0.5O2 Synthetized by Microemulsion, Nanomaterials. 13 (2023) 53. https://doi.org/10.3390/nano13010053.
[43] F. Zhang, C.-H. Chen, J.C. Hanson, R.D. Robinson, I.P. Herman, S.-W. Chan, Phases in Ceria–Zirconia Binary Oxide (1−x)CeO2–xZrO2 Nanoparticles: The Effect of Particle Size, J. Am. Ceram. Soc. 89 (2006) 1028–1036. https://doi.org/10.1111/j.1551-2916.2005.00788.x.
[44] Q. Pan, J. Peng, T. Sun, D. Gao, S. Wang, S. Wang, CO2 methanation on Ni/Ce0.5Zr0.5O2 catalysts for the production of synthetic natural gas, Fuel Process. Technol. 123 (2014) 166–171. https://doi.org/10.1016/j.fuproc.2014.01.004.
[45] P. Topka, M. Klementová, Total oxidation of ethanol over Au/Ce0.5Zr0.5O2 cordierite monolithic catalysts, Appl. Catal. Gen. 522 (2016) 130–137. https://doi.org/10.1016/j.apcata.2016.05.004.
[46] I. Prymak, V. Narayana Kalevaru, S. Wohlrab, A. Martin, Continuous synthesis of diethyl carbonate from ethanol and CO 2 over Ce–Zr–O catalysts, Catal. Sci. Technol. 5 (2015) 2322–2331. https://doi.org/10.1039/C4CY01400F.
[47] P. Fornasiero, J. Kašpar, M. Graziani, On the rate determining step in the reduction of CeO2–ZrO2 mixed oxides, Appl. Catal. B Environ. 22 (1999) L11–L14. https://doi.org/10.1016/S0926-3373(99)00038-7.

[48] J.M. Gatica, R.T. Baker, P. Fornasiero, S. Bernal, G. Blanco, J. Kašpar, Rhodium Dispersion in a Rh/Ce0.68Zr0.32O2 Catalyst Investigated by HRTEM and H2 Chemisorption, J. Phys. Chem. B. 104 (2000) 4667–4672. https://doi.org/10.1021/jp994101z.
[49] P. Fornasiero, J. Kašpar, V. Sergo, M. Graziani, Redox Behavior of High-Surface-Area Rh-, Pt-, and Pd-Loaded Ce0.5Zr0.5O2Mixed Oxide, J. Catal. 182 (1999) 56–69. https://doi.org/10.1006/jcat.1998.2321.
[50] P. Fornasiero, J. Kašpar, M. Graziani, Redox Behavior of High Surface Area Rh-Loaded Ce0.5Zr0.5O2Mixed Oxide, J. Catal. 167 (1997) 576–580. https://doi.org/10.1006/jcat.1997.1593.
[51] C.M. Kalamaras, S. Americanou, A.M. Efstathiou, "Redox" vs "associative formate with –OH group regeneration" WGS reaction mechanism on Pt/CeO2: Effect of platinum particle size, J. Catal. 279 (2011) 287–300. https://doi.org/10.1016/j.jcat.2011.01.024.
[52] E. Baraj, K. Ciahotný, T. Hlinčík, The water gas shift reaction: Catalysts and reaction mechanism, Fuel. 288 (2021) 119817. https://doi.org/10.1016/j.fuel.2020.119817.
[53] M. Zhu, I.E. Wachs, Iron-Based Catalysts for the High-Temperature Water–Gas Shift (HT-WGS) Reaction: A Review, ACS Catal. 6 (2016) 722–732. https://doi.org/10.1021/acscatal.5b02594.
[54] B.S.R. J, M. Loganathan, M.S. Shantha, A Review of the Water Gas Shift Reaction Kinetics, Int. J. Chem. React. Eng. 8 (2010). https://doi.org/10.2202/1542-6580.2238.
[55] S. Saeidi, F. Fazlollahi, S. Najari, D. Iranshahi, J.J. Klemeš, L.L. Baxter, Hydrogen production: Perspectives, separation with special emphasis on kinetics of WGS reaction: A state-of-the-art review, J. Ind. Eng. Chem. 49 (2017) 1–25. https://doi.org/10.1016/j.jiec.2016.12.003.
[56] N. García-Moncada, L. Jurado, L.M. Martínez-Tejada, F. Romero-Sarria, J.A. Odriozola, Boosting water activation determining-step in WGS reaction on structured catalyst by Mo-doping, Catal. Today. 383 (2022) 193–204. https://doi.org/10.1016/j.cattod.2020.06.003.
[57] S. Hilaire, X. Wang, T. Luo, R.J. Gorte, J. Wagner, A comparative study of water-gas-shift reaction over ceria supported metallic catalysts, Appl. Catal. Gen. 215 (2001) 271–278. https://doi.org/10.1016/S0926-860X(01)00535-X.
[58] G. Jacobs, U.M. Graham, E. Chenu, P.M. Patterson, A. Dozier, B.H. Davis, Low-temperature water–gas shift: impact of Pt promoter loading on the partial reduction of ceria and consequences for catalyst design, J. Catal. 229 (2005) 499–512. https://doi.org/10.1016/j.jcat.2004.11.031.
[59] G. Jacobs, L. Williams, U. Graham, G.A. Thomas, D.E. Sparks, B.H. Davis, Low temperature water–gas shift: in situ DRIFTS-reaction study of ceria surface area on the evolution of formates on Pt/CeO2 fuel processing catalysts for fuel cell applications, Appl. Catal. Gen. 252 (2003) 107–118. https://doi.org/10.1016/S0926-860X(03)00410-1.
[60] B. Miao, S.S. Khine Ma, X. Wang, H. Su, S. Hwa Chan, Catalysis mechanisms of CO 2 and CO methanation, Catal. Sci. Technol. 6 (2016) 4048–4058. https://doi.org/10.1039/C6CY00478D.
[61] X. Zhang, N. Rui, X. Jia, X. Hu, C. Liu, Effect of decomposition of catalyst precursor on Ni/CeO2 activity for CO methanation, Chin. J. Catal. 40 (2019) 495–503. https://doi.org/10.1016/S1872-2067(19)63289-4.
[62] C. Mebrahtu, F. Krebs, S. Abate, S. Perathoner, G. Centi, R. Palkovits, Chapter 5 - CO2 Methanation: Principles and Challenges, in: S. Albonetti, S. Perathoner, E.A. Quadrelli (Eds.), Stud. Surf. Sci. Catal., Elsevier, 2019: pp. 85–103. https://doi.org/10.1016/B978-0-444-64127-4.00005-7.
[63] I. Sreedhar, Y. Varun, S. A. Singh, A. Venugopal, B. M. Reddy, Developmental trends in CO 2 methanation using various catalysts, Catal. Sci. Technol. 9 (2019) 4478–4504. https://doi.org/10.1039/C9CY01234F.
[64] A. Jangam, S. Das, N. Dewangan, P. Hongmanorom, W.M. Hui, S. Kawi, Conversion of CO2 to C1 chemicals: Catalyst design, kinetics and mechanism aspects of the reactions, Catal. Today. 358 (2020) 3–29. https://doi.org/10.1016/j.cattod.2019.08.049.

[65] A. Waldvogel, A. Fasolini, F. Basile, S. Thomas, A.-C. Roger, Effect of the Support Synthetic Method on the Activity of Ni/CeZrPr Mixed Oxide in the Co-Methanation of CO2/CO Mixtures for Application in Power-to-Gas with Co-Electrolysis, Energy Fuels. 35 (2021) 13304–13314. https://doi.org/10.1021/acs.energyfuels.1c01524.
[66] I. Champon, A. Bengaouer, A. Chaise, S. Thomas, A.-C. Roger, Carbon dioxide methanation kinetic model on a commercial Ni/Al2O3 catalyst, J. CO2 Util. 34 (2019) 256–265. https://doi.org/10.1016/j.jcou.2019.05.030.
[67] G. Giorgianni, C. Mebrahtu, M.E. Schuster, A.I. Large, G. Held, P. Ferrer, F. Venturini, D. Grinter, R. Palkovits, S. Perathoner, G. Centi, S. Abate, R. Arrigo, Elucidating the mechanism of the CO2 methanation reaction over Ni–Fe hydrotalcite-derived catalysts via surface-sensitive in situ XPS and NEXAFS, Phys. Chem. Chem. Phys. 22 (2020) 18788–18797. https://doi.org/10.1039/D0CP00622J.
[68] P.A.U. Aldana, F. Ocampo, K. Kobl, B. Louis, F. Thibault-Starzyk, M. Daturi, P. Bazin, S. Thomas, A.C. Roger, Catalytic CO2 valorization into CH4 on Ni-based ceria-zirconia. Reaction mechanism by operando IR spectroscopy, Catal. Today. 215 (2013) 201–207. https://doi.org/10.1016/j.cattod.2013.02.019.
[69] J. Ashok, M.L. Ang, S. Kawi, Enhanced activity of CO2 methanation over Ni/CeO2-ZrO2 catalysts: Influence of preparation methods, Catal. Today. 281 (2017) 304–311. https://doi.org/10.1016/j.cattod.2016.07.020.
[70] L. Cornaglia, J. Múnera, E. Lombardo, Recent advances in catalysts, palladium alloys and high temperature WGS membrane reactors: A review, Int. J. Hydrog. Energy. 40 (2015) 3423–3437. https://doi.org/10.1016/j.ijhydene.2014.10.091.
[71] D.I. Slovetskii, E.M. Chistov, Catalytic processes on membrane palladium alloys: I. Carbon monoxide disproportionation, Kinet. Catal. 51 (2010) 255–265. https://doi.org/10.1134/S002315841002014X.
[72] D.B. Schuepfer, F. Badaczewski, J.M. Guerra-Castro, D.M. Hofmann, C. Heiliger, B. Smarsly, P.J. Klar, Assessing the structural properties of graphitic and non-graphitic carbons by Raman spectroscopy, Carbon. 161 (2020) 359–372. https://doi.org/10.1016/j.carbon.2019.12.094.